Fuel 386 (2025) 134248

Contents lists available at ScienceDirect

Fuel

journal homepage: www.elsevier.com/locate/fuel

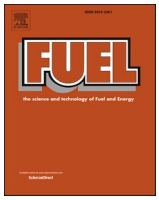

Full Length Article

Insights and applications of biodegradation effects on bitumen chemical compositions and molecular modeling in Athabasca Oil Sands, Canada

Junhao Ren [a], Ningning Zhong [a], Meijun Li [a,b,*], Xiaofa Yang [c], Sibo Yang [d], Bang Zeng [a], Xiaoqiang Liu [b]

[a] National Key Laboratory of Petroleum Resources and Engineering, China University of Petroleum (Beijing), Beijing 102249, China
[b] Faculty of Petroleum, China University of Petroleum-Beijing at Karamay, Karamay 834000, China
[c] Research Institute of Petroleum Exploration and Development, PetroChina, Beijing 100083, China
[d] CNOOC Research Institute Co., Ltd., Beijing 100028, China

ARTICLE INFO

Keywords:
Biodegradation
Bitumen
Chemical composition
Asphaltenes structure
Molecular model

ABSTRACT

In oil sands or heavy oil reservoirs, the chemical compositions and physical properties of fluids often exhibit significant vertical variations within the oil column. These variable properties pose significant challenges for predicting and developing hydrocarbon resources. In this study, the chemical compositions of bitumen at varying biodegradation levels within the oil column of the McMurray Formation in Mackay River area, Athabasca (Canada), were analyzed using extraction of organic matter and fraction separation, gas chromatography-mass spectrometry, elemental analysis, nuclear magnetic resonance hydrogen spectra, X-ray photoelectron spectroscopy, and Fourier transform infrared spectroscopy experiments, to construct bitumen cluster molecular models. The results indicate that with increasing depth of the oil column, the proportion of saturated hydrocarbons decreases, while the resin and asphaltene fractions increase. Compounds with weak biodegradation resistance are largely depleted. Predominantly, the saturated hydrocarbons include terpanes, hopanes, and pregnanes, whereas the aromatic hydrocarbons are rich in methylphenanthrenes, methylchrysenes, and triaromatic steroids. Biodegradation leads to a reduction in the proportion of carbon and hydrogen elements and an increase in heteroatoms within asphaltenes. The chemical structure of asphaltenes is primarily aliphatic, with increasing biodegradation levels, there is an increase in the proportion of H_α and H_β, while H_γ decreases. The degree of condensation and oxygen substitution increases, while the number and length of branched chains, the number of rings per unit structure, and the hydrogen-to-carbon ratio decrease. Biodegradation primarily targets C–H bonds and methylene groups in alkanes and naphthenes, followed by functional groups such as hydroxyl, alcohol, and heteroatoms. This study not only deepens our understanding of the effects of biodegradation on the chemical composition of hydrocarbons but also offers a rapid and cost-effective method for predicting the physical and chemical properties of hydrocarbons.

1. Introduction

The recovery rate for oil sands or heavy oils is highly unstable, the recovery rate of hydrocarbons using Steam Assisted Gravity Drainage (SAGD) technology ranges from 20 % to 55 % [1–3]. This variability can be attributed to two main factors, reservoir heterogeneity and fluid composition variability within the reservoir. Reservoir heterogeneity includes the distribution of muddy interlayers [4,5], petrophysical properties (porosity and permeability) [6,7], petrological characteristics [8–10]. Fluid heterogeneity includes oil or water saturation [11], the spatial distribution of fluids [12], and their physical and chemical characteristics [13].

At the basin scale, the fluid properties of the entire reservoir are influenced by the burial and geothermal histories [14]. Nevertheless, in actual production processes, there is often a greater focus on the heterogeneity of fluids within the oil column. The factor influencing fluid heterogeneity within oil column include: reservoir physical properties [8], oil–water contact surface distribution [11], hydrocarbon fractionation [15], biodegradation [16], as well as thermal alteration and gravity differentiation [13]. Biodegradation is one of the most common

* Corresponding author at: National Key Laboratory of Petroleum Resources and Engineering, China University of Petroleum (Beijing), Beijing 102249, China.
E-mail address: meijunli@cup.edu.cn (M. Li).

https://doi.org/10.1016/j.fuel.2024.134248
Received 11 August 2024; Received in revised form 20 October 2024; Accepted 30 December 2024
Available online 5 January 2025

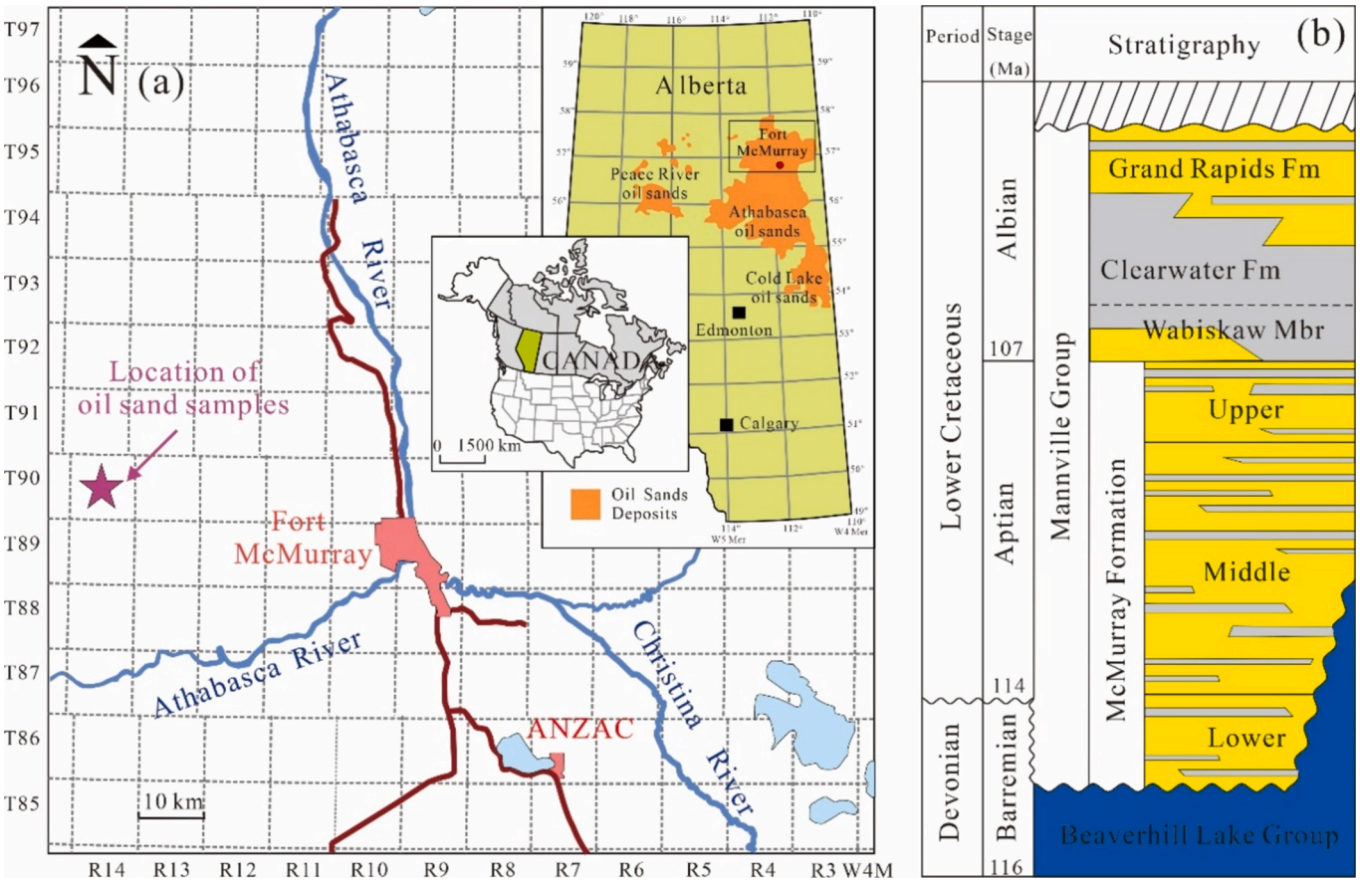

Fig. 1. The location of the Athabasca Mackay River area and the oil column in the Alberta Basin, Canada (modified after [12,42]) (a). The orange area marks the location of the oil sands deposit, and the purple star indicates the position of the sampled oil column. A stratigraphic column of the Athabasca oil sands deposit (b), where yellow indicates sandstone reservoir, grey denotes mudstone, and blue represents carbonate. The oil sands used in this study are primarily sourced from the Upper McMurray Formation.

secondary alteration processes in reservoirs and is a primary mechanism for the formation of heavy oils worldwide [16–18].

The Athabasca oil sands deposit in Canada contains abundant bitumen resources[6,19,20]. The physical properties and chemical composition of bitumen within the reservoir exhibit significant heterogeneity [7,17,21]. Previous research has indicated that biodegradation may be the primary cause of the changes in chemical compositions [13,22,23]. As biodegradation progresses, API values, crude oil mass, and net volume decrease, while density, viscosity, relative content of NSO compounds, and trace metal elements increase [16,24]. In 1993, Peters and Moldowan proposed a scheme to evaluate biodegradation levels based on the varying sensitivities of different compounds, ranging from PM 1 (least degraded) to PM 10 (most degraded) [25]. According to this evaluation method, Athabasca's oil sands bitumen exhibits severe biodegradation levels, ranging from PM 6–9 [12,26]. Larter et al. [27] quantitatively evaluated the biodegradation levels of bitumen through the analysis of naphthalene, phenanthrene, steranes, and hopanes in saturated and aromatics hydrocarbons, accurately fitting the trend of density variation. Zuo et al. [28] employed the Yen-Mullins model to explain the gradual increase in the proportion of asphaltenes during the biodegradation process, which leads to a substantial increase in bitumen viscosity. Therefore, predicting the physical properties of hydrocarbons based on variations in their chemical composition is feasible.

Reports on the chemical structure of Athabasca bitumen are extensive. Early studies utilized infrared spectroscopy to identify the presence of cycloalkanes, sulfur, and nitrogen compounds in bitumen [29]. Results from nuclear magnetic resonance and elemental analysis indicate a high abundance of saturated alkane carbon, and asphaltenes potentially comprising four or more aromatic layers, each containing ten or more aromatic rings [30,31]. Based on organic chemistry and thermal degradation experimental data, various average molecular structures for Athabasca asphaltenes have been proposed, including island model [31–33] and archipelago [34–36] model. Murgich et al. [33] demonstrated through molecular mechanics that the formation of bitumen micelles is due to the interactions between aromatic layers, a perspective further supported by the subsequent Yen-Mullins aggregation model [37,38]. Given the complex chemical structure of bitumen, constructing molecular models combined with molecular dynamics simulations has become a key method for predicting its physical properties [39–41].

However, research on the chemical composition of bitumen at different levels of biodegradation remains limited. Predicting the physical properties of hydrocarbon fluids at the oil column scale continues to pose substantial challenges. This study aimed to investigate the effects of biodegradation on the saturated and aromatic hydrocarbons compounds, chemical structure of asphaltenes within oil column through experimental analysis using gas chromatography-mass spectrometry (GC–MS), elemental analysis, X-ray photoelectron spectroscopy (XPS), nuclear magnetic resonance hydrogen spectra (^{1}H NMR), and Fourier transform infrared spectrometer (FTIR). Meanwhile, constructing precise molecular models can the quickly and accurately simulate and predict the physical and chemical properties of heavy oil or bitumen.

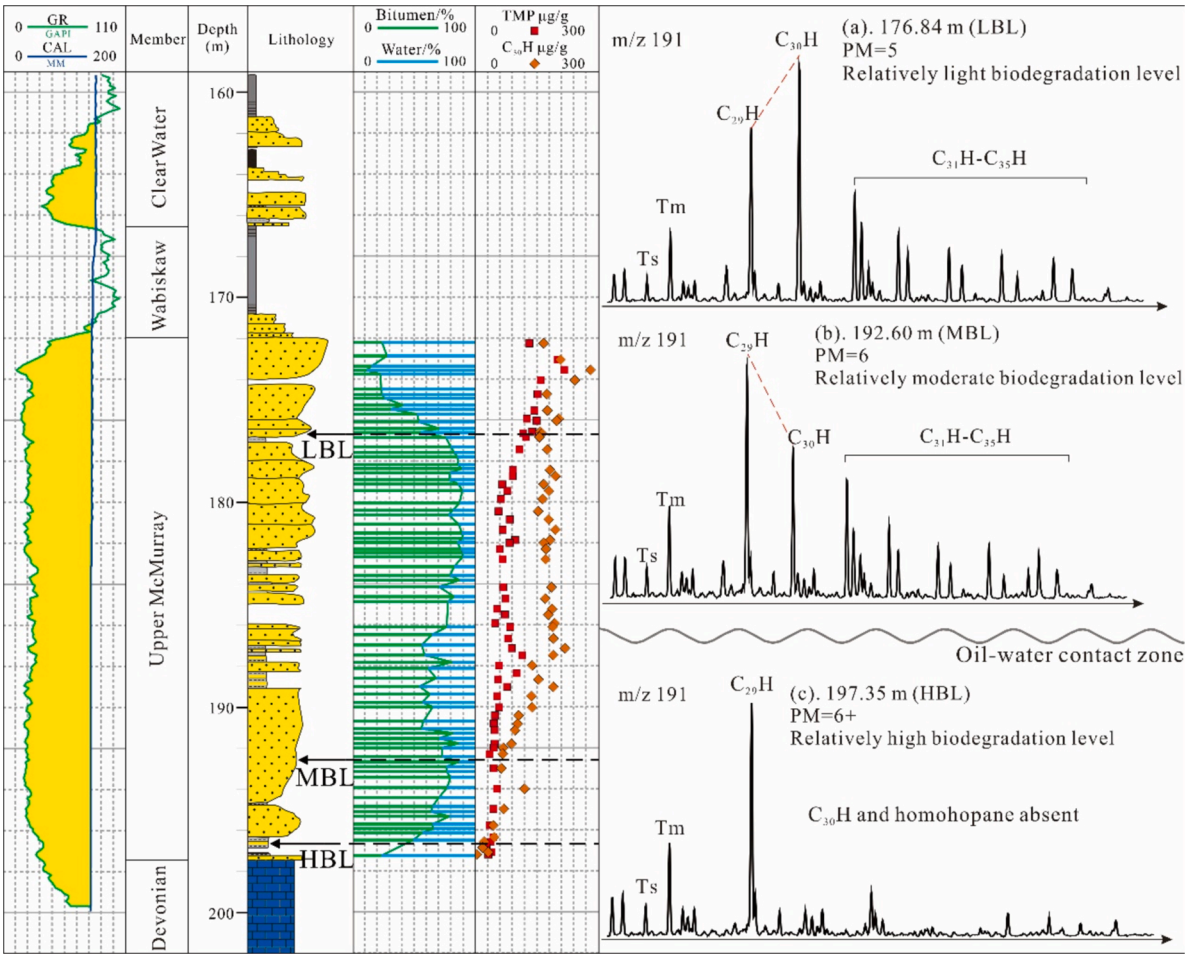

Fig. 2. There are significant differences in the oil saturation with the oil column, and the concentration of certain compounds in saturated and aromatic fractions varies in a gradient, which may be caused by differences in biodegradation levels. According to the evaluation criteria of Peters and Moldowan [25], the relative concentration of hopanes decreased sequentially in the oil sand samples as biodegradation levels increased (PM 5–6). LBL: relatively light biodegradation level, MBL: relatively moderate biodegradation level, HBL: relatively high biodegradation level. TMP: trimethylphenes, C_{30} H: C_{30} hopanes.

Table 1
The differences in bitumen content and group composition of oil sands at varying levels of biodegradation in the Mackay River area.

Sample	Depth/m	Biodegradation level	Bitumen/% Wt	Sat/%	Aro%	Res/%	Asp/%	(Sat + Aro)/(Res + Asp)
LBL	176.84	PM 5	14.93	24.47	30.65	18.17	26.71	1.23
MBL	192.6	PM 6	6.12	22.51	20.88	24.67	31.94	0.77
HBL	197.35	PM 6+	4.68	18.05	23.46	24.76	33.73	0.71

Sat: mass percentage of saturated hydrocarbon; Aro: mass percentage of aromatics hydrocarbon; Res: mass percentage of resin; Asp: mass percentage of asphaltene.

2. Materials, experiments, and simulation method

2.1. Materials

The oil sands resources of Canada's Alberta Basin are mainly distributed in Athabasca, Pease River, and Cold Lake (Fig. 1a orange part) [42]. Oil sand reservoirs are primarily located in the McMurray Formation (Fig. 1b bright yellow part) of the Cretaceous Mannville Group, which is informally divided into the upper, middle, and lower three members [43]. The reservoir lithology is dominated by fine sandstone and contains many muddy interlayers (Fig. 1b gray part) ranging in thicknesses from centimeters to meters.

The Mackay River area is situated approximately 35 km northwest of Fort McMurray in the Athabasca region, with oil sand reservoirs mainly found in the Upper McMurray Member. An oil column with a thickness of 26 m (Fig. 2) was selected in the Mackay River area and buried at a depth of 172–198 m.

Gradient variations in bitumen contents and chemical compositions attributed to differences in the biodegradation levels within the oil column have been mentioned in numerous reports [7,23]. Therefore, three oil sand samples with increasing levels of biodegradation were selected from the top to bottom within the oil column. These samples were taken at depths of 176.84 m, 192.6 m, and 197.35 m, respectively. According to their biodegradation levels, they are named LBL (relatively light biodegradation level), MBL (relatively moderate biodegradation level), and HBL (relatively high biodegradation level); the sampling locations were marked by arrows (Fig. 2).

2.2. Experiment

2.2.1. Extraction and separation of organic matter

Extraction and separation of organic matter from oil sands by organic

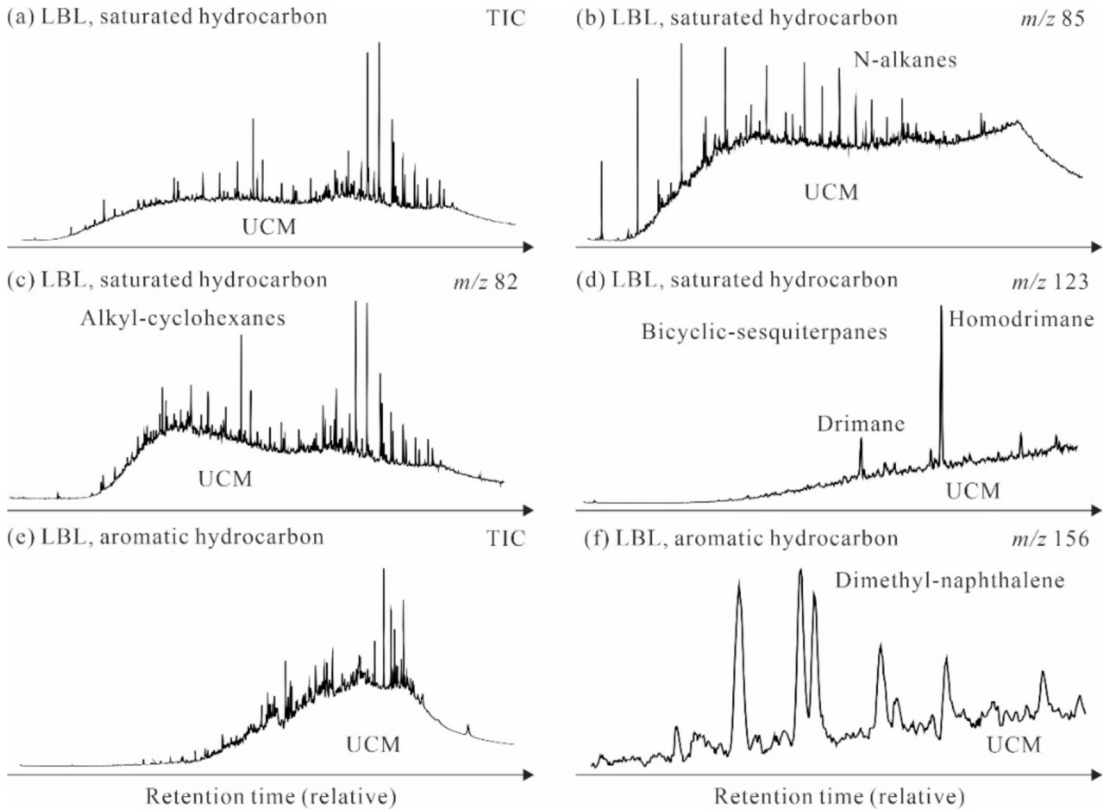

Fig. 3. Due to severe biodegradation, the baseline of the total ion chromatogram (TIC) (a) (c) of saturated and aromatic hydrocarbon in the LBL sample has been uplift, exhibiting a UCM (unresolved complex compounds) 'hump'. The mass chromatograms *m/z* 85 (b), *m/z* 82 (c), and *m/z* 123 (d) represent n-alkanes, alkyl-cyclohexanes, and bicyclic-sesquiterpanes in saturated hydrocarbons. The mass chromatograms *m/z* 156 (f) represent dimethylnaphthalenes in aromatics hydrocarbons. Severe biodegradation results in these compounds with weak resistance to biodegradation below the detection limit.

solvent, performing standard reference SY/T 5119–2016. About 5 g of fresh oil sand is cut with a clean knife, wrapped in filter paper and degreasing cotton, and then subjected to Soxhlet extraction for 72 h using dichloromethane as the solvent. The weight of extracted organic matter represents the bitumen content of the oil sand. The extracted bitumen is first mixed with petroleum ether and precipitated to separate asphaltene. Subsequently, the maltene fraction is separated using a mixture of petroleum ether and dichloromethane in varying proportions. The fractions of saturated hydrocarbons, aromatic hydrocarbons, and resins are sequentially separated, and their proportions are measured. For details of the separation process, refer to previous reports [44].

2.2.2. Saturated and aromatic hydrocarbons gas chromatography-mass spectrometry

GC–MS analysis enables the identification of low-concentration compounds and provides molecular weight and structural information of these compounds. Combined with standard samples, it facilitates quantitative analysis. The execution standard can be referred to in GB/T 18606–2017. The abundances of various compounds in saturated and aromatic hydrocarbons were analyzed using a GC–MS system (Agilent 6890 GC-5975i MS). The column used was an HP-5MS elastic quartz capillary tube, with an injection temperature maintained at 300℃. Pure helium served as the carrier gas at a flow rate of 1 mL/min. The ionization mode was EI with an ionization energy of 70 eV. Detailed experimental procedures can be found in the relevant literature [45]. For standards, 0.2 μg of deuterated C_{29} steranes and deuterated dibenzothiophene were used in both saturated and aromatic hydrocarbons. The absolute content of each compound was calculated by integrating the area under the corresponding peaks.

2.2.3. Chemical structure analysis of asphaltenes

NMR spectroscopy is a widely used technique for elucidating the chemical structure of asphaltenes, providing detailed information on the environment and distribution of hydrogen atoms and aiding in the assessment of their properties and changes. To distinguish between different types of hydrogen atoms (aromatic or aliphatic hydrogen), quantitative information on the chemical structure of asphaltene was obtained. Asphaltene fractions in solution were measured using the AVANCE III HD (400 MHz) nuclear magnetic resonance spectrometer from Bruker Germany. The execution standard can be referred to in SY/T 5777–2022. The spectra were recorded at 400 MHz using a 5 mm broadband probe. Dichloromethane was used as the solvent, and spectral analysis corrected for its peak effect. Deuterated chloroform ($CDCl_3$) served as the solvent for recording, with tetramethylsilane (TMS) as the internal standard. Chemical shifts in the spectra were referenced to the residual proton signal of $CDCl_3$ at 7.26 ppm. Experiments were conducted under dust-free conditions at 25 °C, with a spectral width of 10.0 kHz, RF pulse of 3.3 μs, acquisition time of 2.5 s, and 256 accumulations. Gaussian function fitting of the spectra was performed using Peakfit software, following previous reports on asphaltene structure chemical shifts [30,46]. To ensure fitting accuracy, an average of 100 sub-peaks was used, maintaining consistent sub-peak widths throughout the analysis.

XPS are commonly used methods for analyzing the elemental composition of unknown compounds. The relative changes in each element and chemical structure within asphaltene were analyzed using X-ray photoelectron spectroscopy. The execution standard can be referred to in GB/T 25184–2010. The equipment adopts the K-Alpha Kα ray photoelectron spectrometer of Thermo Fisher Scientific in the UK. The instrument used monochromatic aluminum Kα radiation with an excitation energy of 1468.6 eV. The X-ray spot size was set to 400 μm,

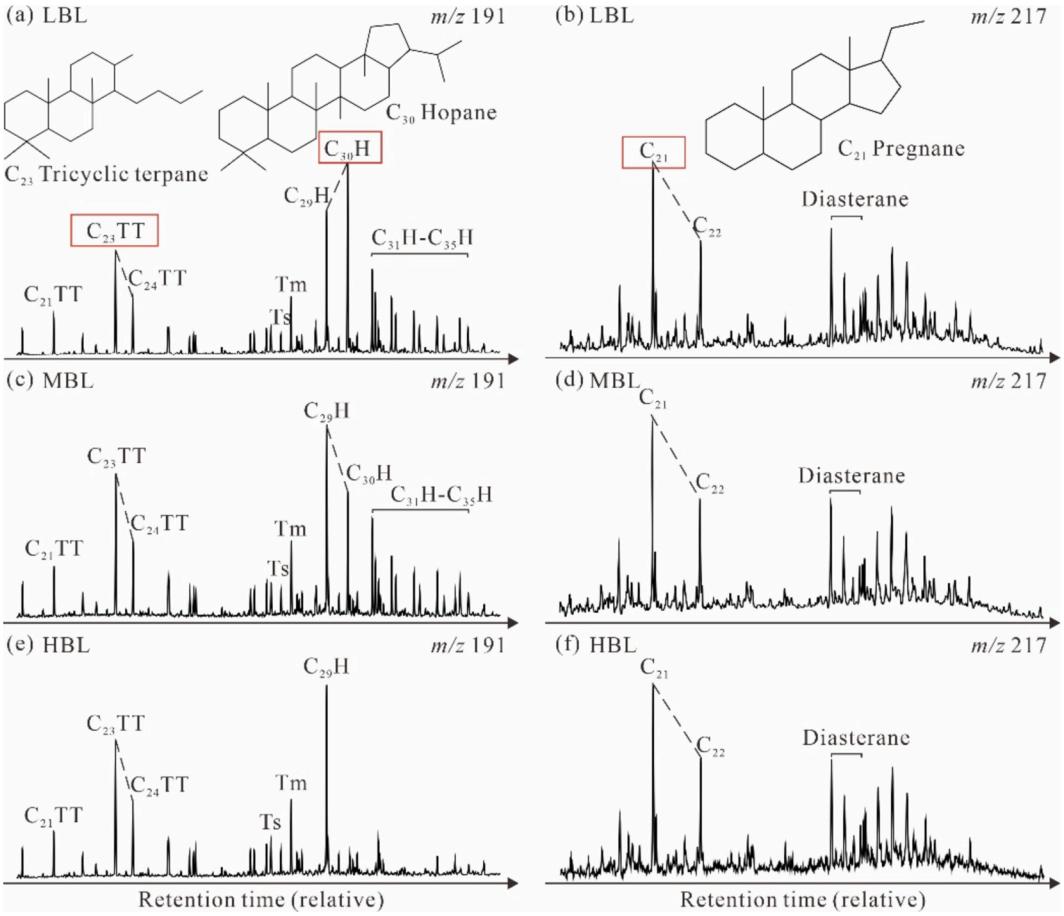

Fig. 4. The saturated hydrocarbon mass chromatograms *m/z* 191 and *m/z* 217 exhibit higher abundances of C_{23} TT, C_{30} H, and C_{21} pregnane, which can be considered representative compounds of saturated hydrocarbons. Additionally, C_{30} H shows a negative correlation with biodegradation levels. TT: tricyclic terpanes; H: hopanes; Ts: 18α(H)-trisnorneohopane; Tm: 17α(H)-trisnorneohopane.

and the spectrum acquisition range was 0–1350 eV. A wide scan was conducted at 100 eV, followed by high-resolution single-element spectra acquired at 30 eV with an energy step of 0.1 eV. The carbon element signal at 283 eV was selected for binding energy calibration. Avantage software was employed to identify and fit the binding energies of carbon (C), nitrogen (N), and sulfur (S) elements. Chemical structures characterized by different energy signals were referenced from the previous reports [47].

The percentage of C, H, O, N and S in the asphaltene fraction was analyzed by using the Elementar Vario EL cube CHNSO element analyzer. The execution standard can be referred to in GB/T 19143–2017. Approximately 20–40 μg of asphaltene samples were weighed, wrapped in tin cups, and placed in an automatic tray. Finally, helium was used as a carrier gas to enter the TCD detector for analysis.

FTIR is capable of identifying characteristic absorption peaks of different functional groups within complex mixtures. The functional groups and their relative proportions in the asphaltenes were identified using a Bruker Vertex 70v spectrometer. The execution standard can be referred to in SY/T 5121–2021.The potassium bromide and asphaltene samples were mixed thoroughly at a mass ratio of 1:100. A pressure of 13 MPa was applied using a hydraulic press for 5 min to create circular tablets with a diameter of no more than 10 mm. The scan was performed with a resolution of 4 cm^{-1} in the wave number range of 4000–400 cm^{-1}.

2.3. Methods of model construction

A classic four-component method involving asphaltenes, resin, aromatic, and saturated hydrocarbons was used to establish a bitumen model. The absolute content of compounds in saturated and aromatic hydrocarbon fractions was identified and quantified using GC–MS results, focusing on compounds with relatively high content and representativeness. The chemical structure of asphaltene fractions was analyzed by elemental analysis, ^{1}H NMR, XPS, and FTIR results, which provided basic information for the construction of the molecular model. Two-dimensional molecular models were drawn and analyzed in ChemDraw software. Subsequently, they were optimized, assembled, and dynamically tested using Material Studio software. To ensure the reliability of the model, the model optimization process was adopted by Liu et al [48]. Geometric optimization was initially performed using the COMPASS force field [49] to minimize the overall energy and obtain reasonable cell parameters. The Smart method algorithm was employed with energy set at 2.0×10^{-5} kcal/mol, and a maximum of 5×10^6 iterations. Afterward, the NPT ensemble was annealed at 298.15 K, 0.1 MPa (simulated normal temperature and pressure). Temperature and pressure were controlled using the Nose-Hoover and Berendsen methods to achieve thermodynamic equilibrium and attain the most reasonable spatial configuration for the model.

3. Results

3.1. Biodegradation levels in the oil column

The bitumen content and relative proportions of the four components in oil sand samples are shown in Table 1. The bitumen content of the LBL, MBL, and HBL oil sand samples decreased sequentially by

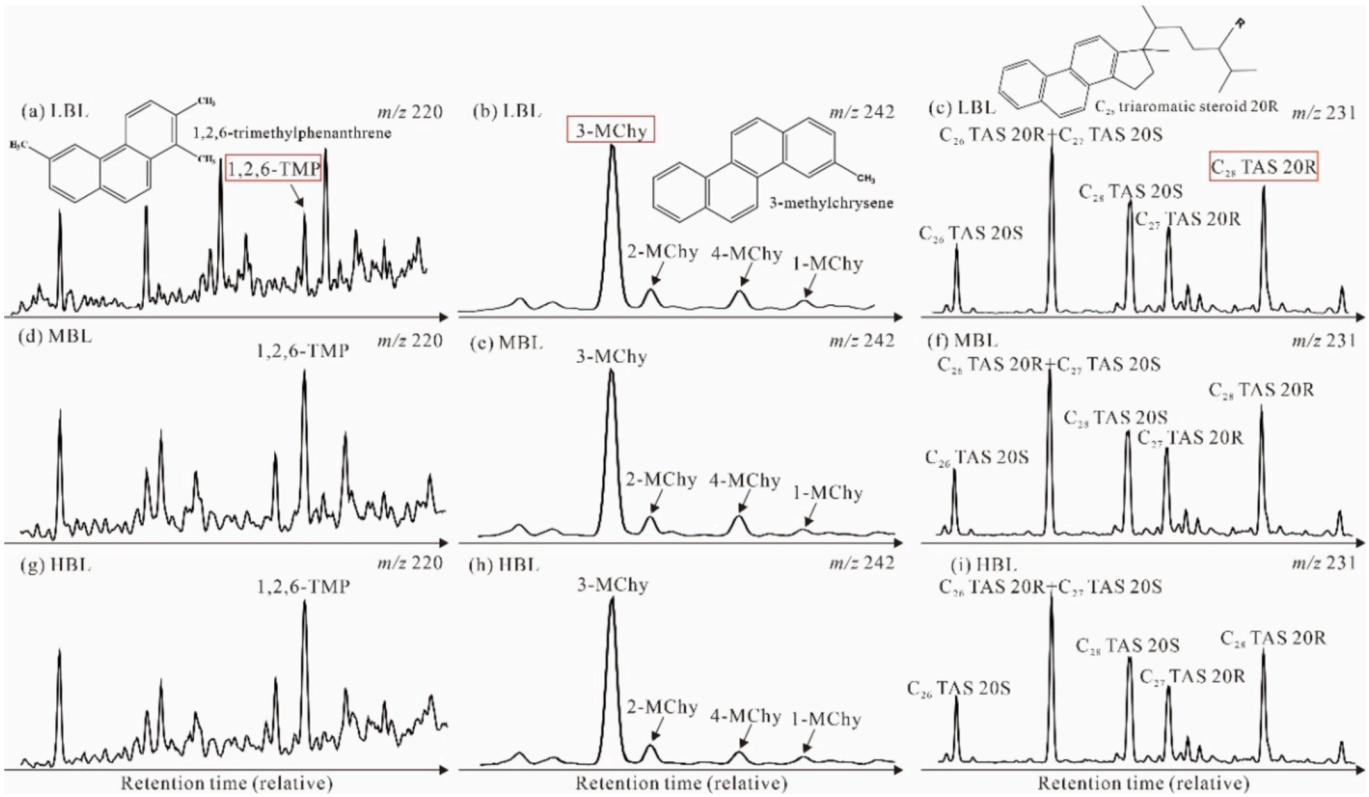

Fig. 5. The aromatics hydrocarbon mass chromatograms of three oil sand samples, *m/z* 220, *m/z* 242, and *m/z* 231, show relatively high abundances of 1, 2, 6-TMP, 3-MChy, and C_{28} TAS 20R. These compounds, with strong resistance to biodegradation and containing more than three rings, can serve as representative compounds in aromatics hydrocarbon. 1, 2, 6-TMP: 1, 2, 6-trimethylphenanthrene; MChy: methylchrysene; TAS: triaromatic steroid.

Table 2
The differences in elemental composition of bitumen at varying levels of biodegradation.

Sample	C/wt%	H/wt%	O/wt%	N/wt%	S/wt%	H/C	O/C	N/C	S/C
LBL	81.37	8.83	2.89	0.48	6.43	0.11	0.04	0.01	0.08
MBL	80.62	8.48	3.50	0.57	6.83	0.11	0.04	0.01	0.08
HBL	79.55	7.28	4.88	0.67	7.62	0.09	0.06	0.01	0.10

14.93 %, 6.12 %, and 4.68 %, respectively. Additionally, with increasing depth, the proportion of saturated hydrocarbons in bitumen decreased from 24.47 % to 18.05 %, while the proportion of asphaltene increased from 26.71 % to 33.73 %. The ratio of saturated plus aromatic hydrocarbons to resin plus asphaltenes can reflect the change of light and heavy bitumen fraction (0.71–1.23). The bitumen content shows a negative correlation with the resin plus asphaltenes fraction. Even within the same oil column, there can be significant differences in the content and composition of bitumen.

The variation in the relative abundance of compounds in saturated and aromatic hydrocarbons can be used to identify the difference in biodegradation levels. The absolute content of C_{30} hopanes (C_{30}H) and trimethylphenanthrene (TMP) compounds decreased with increasing depth, showing a positive correlation with the biodegradation levels. (Fig. 2).

For the LBL sample, the saturated hydrocarbons mass chromatogram *m/z* 191, the compounds of 18α-C_{27} trisnorhopane (Ts), 17α-C_{27} trisnorhopane (Tm), and C_{31} homohopane–C_{35} homohopane (C_{31}H–C_{35}H) remained intact. The relative abundance of C_{30}H is higher than that of C_{29} hopane (C_{29}H). According to the identification criteria of PM biodegradation levels, the hopanes may have just begun to degrade, and the biodegradation level is PM 5 (Fig. 2a). For the MBL samples, the relative abundance of C_{30}H in the saturated hydrocarbons is lower than that of C_{29}H, indicating that the hopanes has suffered substantive losses and the biodegradation level reaches PM 6 (Fig. 2b). In the HBL samples, both compounds of C_{30}H and C_{31}H–C_{35}H were below the detection limits. Due to the strong resistance to biodegradation of Ts and Tm compounds, they usually remain unaffected until PM 8 or higher. The complete absence of C_{30}H suggests that the biodegradation level may have exceeded PM 6 (Fig. 2c).

3.2. Characteristics of saturated and aromatic hydrocarbons

As mentioned above, the LBL samples have the lowest biodegradation levels among the three samples, allowing for a relatively comprehensive analysis of the abundance of compounds in LBL samples. The baseline of the total ion chromatogram (TIC) for saturated and aromatic hydrocarbons is uplifted and shows a 'hump' of unresolved complex compounds (UCM) (Fig. 3a, e) [24,25]. Severe biodegradation may render most hydrocarbons with weaker resistance to biodegradation unrecognizable.

The *m/z* 85, *m/z* 82, and *m/z* 123 of the mass chromatogram represent the n-alkanes, alkyl-cyclohexanes, and bicyclic-sesquiterpanes in LBL saturated hydrocarbons (Fig. 3b, c, d). The identification results indicate that the abundance of these compounds is below the detection limit, hence they are not representative of saturated hydrocarbons. The mass chromatogram peak at *m/z* 156 represents the dimethylnaphthalenes in aromatic hydrocarbons, where the low abundance

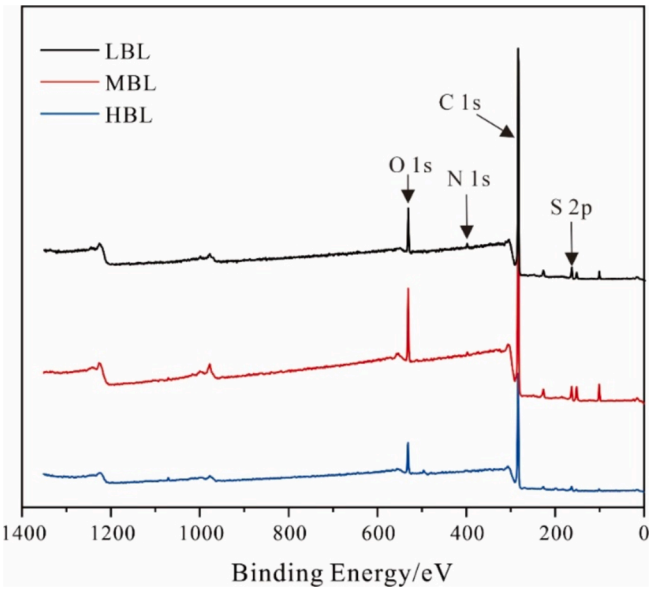

Fig. 6. X-ray photoelectron spectroscopy of asphaltenes from three different biodegradation levels of oil sands bitumen reveals that carbon is the most abundant element, while the proportions of oxygen, nitrogen, and sulfur show variations. Identified the binding energy range and relative proportions of four elements: carbon (C), oxygen (O), nitrogen (N), and sulfur (S).

Table 3
The analysis of XPS data reveals the differences in the proportions of various elements in asphaltenes at different levels of biodegradation.

Element	LBL		MBL		HBL	
	Binding energy/ eV	Atomic/ %	Binding energy/ eV	Atomic/ %	Binding energy/ eV	Atomic/ %
C 1 s	283.87	84.18	283.11	83.63	283.23	83.09
O 1 s	531.16	7.28	530.85	8.89	531.05	10.73
N 1 s	398.81	1.4	398.65	1.64	398.74	2.77
S 2p	163.24	2.58	162.54	2.67	162.54	2.88
Other		4.56		3.17		0.53

indicates aromatic compounds less than three rings are affected by biodegradation and are also not representative (Fig. 3f).

The absolute content of each compound type was calculated by adding the standard samples of saturated and aromatic hydrocarbons, and their relative mass proportions were determined based on the total detectable biomarkers [24], then representative compounds were selected. In saturated hydrocarbons, terpanes, hopanes, and pregnanes are dominant, with hopanes showing significant differences due to the impact of biodegradation (Fig. 2). Among them, C_{23} tricyclic terpanes (C_{23}TT), C_{30}H, and C_{21} pregnane are the most abundance compounds in their respective series (Fig. 4). In aromatics, mass chromatograms at *m/z* 220, *m/z* 242, and *m/z* 231 highlight the relative abundance of trimethylphenanthrenes, methylchrysenes, and triaromatic steroids containing at least three rings. Among these, 1, 2, 6-trimethylphenanthrene (1, 2, 6-TMP), 3-methylchrysene (3-MChy) and C_{28} triaromatic steroids 20R (C_{28} TAS 20R) are the most abundant compounds in their respective series (Fig. 5) (Some peaks of co-elution compounds are not considered).

3.3. Asphaltene structural features

Asphaltene is generally considered a mixture of the largest molecular weight and extremely complex chemical structure of crude oil components, usually containing heteroatoms such as nitrogen, oxygen, sulfur, and small amounts of metal elements [30]. Asphaltene characteristics are one of the important factors affecting the physical and chemical properties of crude oil. Therefore, the detailed analysis of asphaltene structure is helpful to further understanding the molecular scale characterization of bitumen with different biodegradation levels. Currently, the average molecular structure model is an effective method to characterize the chemical structure of asphaltenes, which usually relies on experimental data to establish basic structural insights [39].

3.3.1. Elemental composition and XPS analysis

The elemental mass percentage analysis of asphaltenes is shown in Table 2. Metal elements are not included in the scope of the experiment. The carbon content in asphaltenes is the highest, ranging from 79.55 % to 81.37 %, whereas the nitrogen content is the lowest, averaging less than 1 %. The ratio of hydrogen to carbon (H/C) decreased with the increase of biodegradation level (0.11–0.09), while the ratio of oxygen to carbon (O/C, 0.04–0.06) and the ratio of sulfur to carbon (S/C, 0.08–0.10) increased with the increase of biodegradation level. With a higher biodegradation level, there is a decrease in the relative proportion of carbon and hydrogen elements, and an increase in heteroatoms such as nitrogen, oxygen, and sulfur.

The specific types and contents of carbon, oxygen, nitrogen, and sulfur elements in asphaltene were further analyzed through the XPS experiments, and the range of binding energy is referred to in the previous relevant reports [47]. The positions of each element were marked on the original XPS spectrogram of the three asphaltenes (Fig. 6). Elemental peaks and corresponding peak intensities were identified and measured by software [50], and the analysis results were shown in Table 3. The highest intensity peak corresponds to a relative proportion of carbon ranging from 83.09 % to 84.18 %, with a combined energy of approximately 283 eV. The identification peak of oxygen usually appears at the binding energy of 531 eV, constituting the second largest component ranging from 7.28 % to 10.73 %. Nitrogen was identified around 398 eV, comprising 1.4 % to 2.77 % of the composition. Sulfur, with a peak at about 162 eV, accounted for 2.58 % to 2.88 %.

The remaining unidentified elements, potentially including metal and chlorine elements introduced during processing, are uniformly classified as other elements, with a relative proportion of 0.53 % to 4.56 %. These elements are not regarded as the main object of concern. The biodegradation level shows a negative correlation with the proportion of carbon elements and a positive correlation with the proportions of nitrogen, oxygen, and sulfur elements.

The forms of carbon, oxygen, nitrogen, and sulfur elements were further analyzed through the scanning results of the high-resolution spectrum. Due to the interference of nitrogen and sulfur elements with the accuracy of oxygen peaks during the scanning process, carbon spectroscopy was used to analyze the binding modes of carbon and oxygen [51]. The spectrum shows that carbon peaks dominate in these three asphaltenes, identifying the binding energy range of 282–290 eV. The sulfur peak binding energy is identified in the range of 160 to 170 eV. The abundance of nitrogen is low, and its peak pattern exhibits significant fluctuations, ranging from 396 to 402 eV. High-resolution scanning signals of carbon, oxygen, nitrogen, and sulfur elements were peak-fitted for asphaltene samples with three different biodegradation levels, enabling analysis of their respective chemical structures (Fig. 7).

As shown in Table 4, the fitting results of function show that carbon and oxygen mainly include aliphatic and aromatic carbon, C-O, O = C-O, and O = C. Aliphatic and aromatic carbon account for 88.66 %-93.26 % and are the most dominant carbon structures. The proportion of O = C ranges from 4.59 % to 6.86 %, slightly higher than the content of C-O and O = C-O. With the increase in biodegradation level, the proportion of C-O, aliphatic, and aromatic carbon decreased. Due to the low abundance of nitrogen elements, only two types of pyridine and pyrrole are identified. Most nitrogen elements in asphaltene exist as pyrrole, with a relative proportion ranging from 89.89 % to 94.24 %. As the biodegradation level increases, the proportion of pyrrole in asphaltene decreases, and the proportion of pyridine increases.

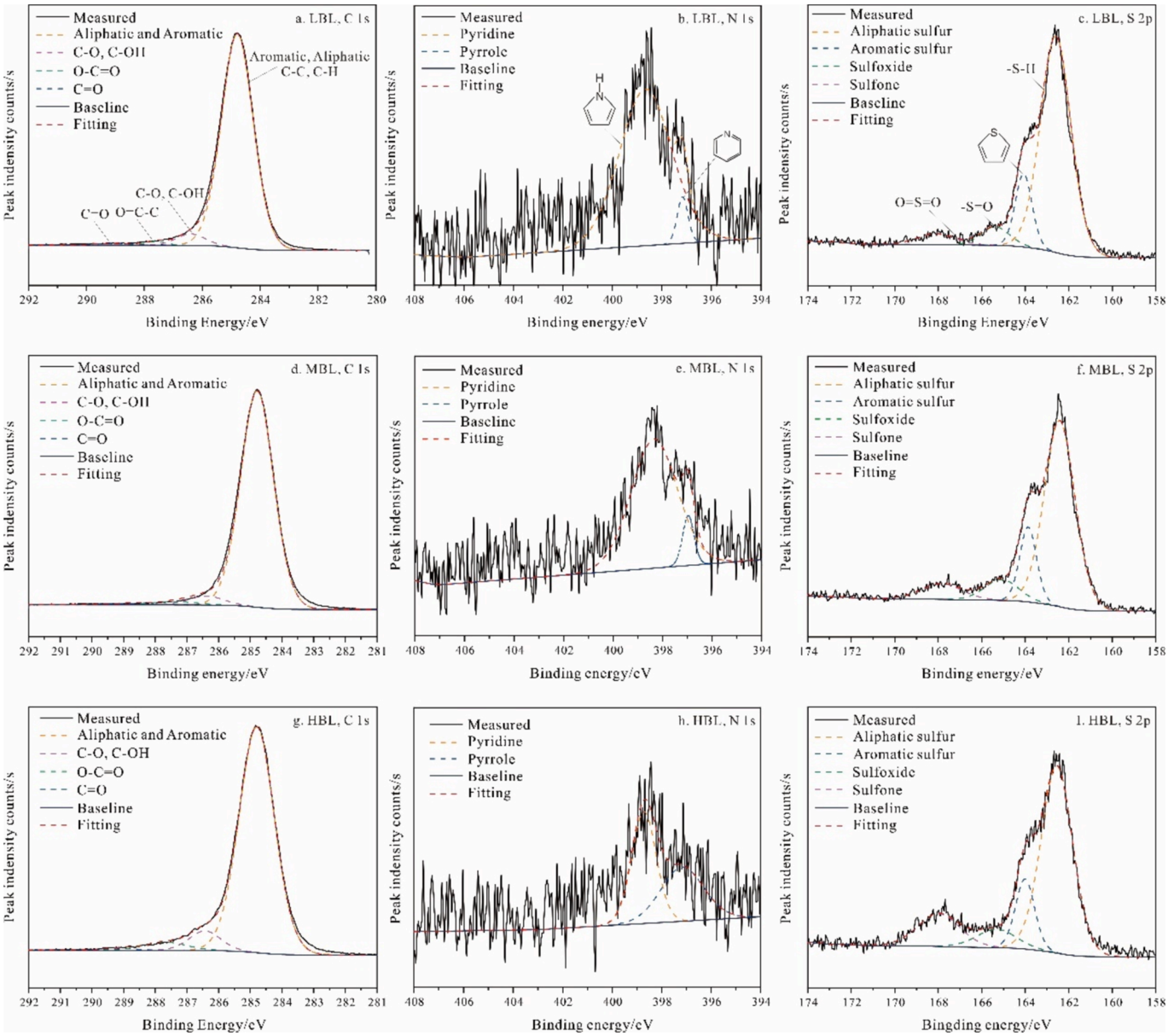

Fig. 7. Peak hitting of high-resolution X-ray photoelectron spectroscopy was used to identify the forms of carbon, oxygen, nitrogen, and sulfur in asphaltenes at different levels of biodegradation. Carbon and oxygen are primarily found in aliphatic and aromatic forms, while nitrogen is categorized into pyridine and pyrrole types, with sulfur mainly existing in an aliphatic form.

Table 4
Analysis of elemental forms in asphaltenes at different levels of biodegradation using high-resolution XPS scanning results. Biodegradation results in an increase in structures related to nitrogen, oxygen, and sulfur, while structures associated with aliphatic and aromatic compounds decrease.

Elemental peak	Functionality	LBL		MBL		HBL	
		Binding energy/eV	Atomic/%	Binding energy/eV	Atomic/%	Binding energy/eV	Atomic/%
C 1 s and O 1 s	Aliphatic and aromatic	284.80	93.26	284.80	92.45	284.80	88.66
	C-O and C-OH	289.02	1.10	289.00	0.85	289.13	0.65
	O = C-O	287.60	1.05	287.36	1.79	287.68	3.83
	O = C	286.39	4.59	286.39	4.91	286.43	6.86
N 1 s	Pyridine	397.15	5.76	396.97	7.54	397.12	10.11
	Pyrrole	398.78	94.24	398.32	92.46	398.38	89.89
S 2p	Aliphatic sulfur	162.61	74.85	162.42	68.47	162.55	63.22
	Aromatic sulfur	164.07	14.26	163.86	15.23	164.01	15.29
	Sulfoxide	165.39	6.19	165.08	8.56	165.33	8.84
	Sulfone	168.08	4.70	167.84	7.74	167.97	12.65

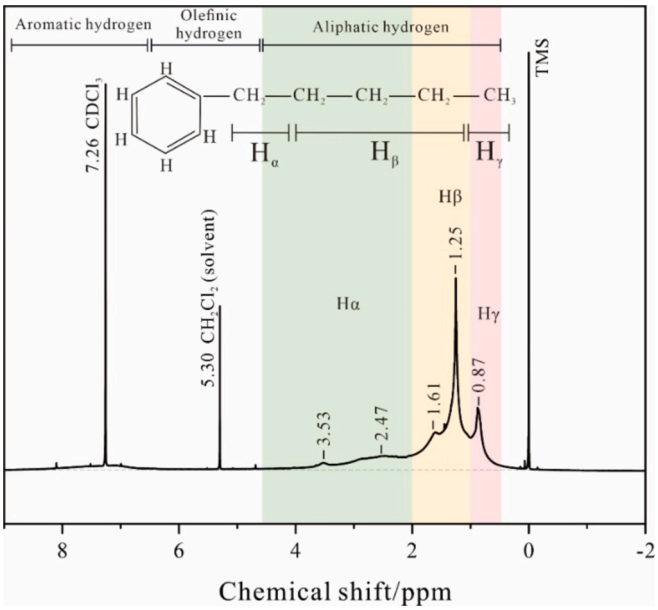

Fig. 8. The ^{1} H NMR spectra of asphaltene in LBL oil sand bitumen, TMS is tetramethylsilane (internal standard), $CDCl_3$ is deuterated chloroform (solvent), and $CHCl_2$ is dichloromethane (solvent). 0.5–4.5 ppm is the chemical shift of aliphatic hydrogen, which can be identified as H_α (green region), H_β (yellow region), and H_γ (red region) based on the link distance to the aromatic ring.

The sulfur element in asphaltenes is identified into four types: aliphatic sulfur, aromatic sulfur, sulfoxide, and sulfone. The proportion of aliphatic sulfur ranges from 63.22 %–74.85 %, and the proportion of aromatic sulfur ranges from 14.26 %–15.29 %, both being the main sulfur structures. The proportion of sulfone and sulfoxide is relatively small, except for the HBL samples, where the relative proportion of sulfoxide is greater than sulfone. The biodegradation level is negatively correlated with the proportion of aliphatic sulfur and positively correlated with other sulfur structures, with the relative proportion of sulfone increasing rapidly.

3.3.2. ^{1}H NMR analysis

The ^{1}H NMR of LBL samples was used as a typical case, and the analytical process same as the other two samples. Chemical shifts of 0 ppm, 5.30 ppm and 7.26 ppm correspond to the peaks of the TMS internal standard, dichloromethane solvent and $CDCl_3$ solvent, respectively, which are not included in the analysis process. The identification range of the hydrogen spectra can be roughly divided into three ranges: aliphatic hydrogen (0.1–4.5 ppm), olefinic hydrogen (4.5–6.0 ppm), and aromatic hydrogen (6.0–9.0 ppm) [30,52]. The original hydrogen spectra show that asphaltenes contain a rich amount of aliphatic hydrogen and a small amount of aromatic hydrogen (0.07 %–0.14 %), with almost no olefinic hydrogen (Fig. 8). Therefore, the difference between the three asphaltenes is mainly reflected in the distribution range of aliphatic hydrogen. According to the connection distance with the aromatic ring, the types of aliphatic hydrogen can be divided into H_γ (0.1–1.0 ppm, red region), H_β (1.5–2.0 ppm, yellow region), and H_α (2.0–4.5 ppm, green region) in order (The simplified molecular structure highlights the distribution of different types of hydrogen atoms).

The chemical shift signals in the range of 0–5 ppm of the spectra was intercepted for fine comparison. The hydrogen spectral peak patterns were integrated by using Gaussian fitting to calculate the proportions of different types of hydrogen in the three asphaltenes (Fig. 9). The fitting degree of three asphaltenes showed an average R^2 value of 0.996, demonstrating the reliability of the peak fitting results. The H_β and H_α were further divided into $H_{\beta\text{-}1}$, $H_{\beta\text{-}2}$, $H_{\alpha\text{-}1}$, and $H_{\alpha\text{-}2}$ according to the differences in chemical shifts, resulting in the identification of six types of hydrogen. The description and fitting statistical results of the kinds of hydrogen atoms are shown in Table 5 [46]. The hydrogen in the three asphaltenes is mainly provided by the methylene at the β position of paraffin and naphthenes, with a relative proportion of 59.9 %–60.76 %. The proportion ranges of H_γ and H_α are 14.50 %–20.27 % and 19.76 %–24.08 %, respectively. The proportion of hydrogen in the methyl and methylene directly connected with paraffin or naphthene is slightly higher than that in the methyl at the end of the chain or paraffin. In addition, the biodegradation level is negatively correlated with the proportion of H_γ, $H_{\beta\text{-}2}$, and $H_{\alpha\text{-}1}$, and positively correlated with the proportion of $H_{\beta\text{-}1}$, $H_{\alpha\text{-}2}$, and H_{ar}.

The structural parameters of asphaltene were calculated by the improved B-L method combined with the elemental analysis and ^{1}H NMR analysis results [53,54]. The structural parameters and calculation equations are shown in Appendix Table S1. The aromatic carbon ratio (f_{ar}) of the three asphaltenes ranged from 0.40 to 0.43 and was negatively correlated with the biodegradation level. In addition, the H_{au}/C_{ar} value is inversely proportional to the condensation degree of the chemical structure, which is often used to characterize the condensation degree of the aromatic rings [54]. The results showed that H_{ar}/C_{ar} values ranged from 0.30 to 0.39, and the biodegradation level is positively correlated with the degree of condensation of asphaltene. Furthermore, the σ_o value is commonly used to evaluate the oxidation degree of chemical structure, which increased from 0.22 to 0.29 as the biodegradation level increased.

The relevant parameters of carbon structure, including $C_{n(us)}$, $C_{al(us)}$, $C_{ar(us)}$, and $C_{p(us)}$, were used to characterize naphthenic carbon, aliphatic carbon, aromatic carbon and aromatic peripheral carbon in the asphaltene structure. The calculated results showed that these carbon structures decreased with the increase of biodegradation level, which is consistent with the experimental results of the element analysis. The range of L values can be used to evaluate the average branched chain length of the structure. With the increase of biodegradation level, the L value decreases from 0.29 to 2.0, indicating a reduction in the average branched chain length.

3.3.3. FTIR analysis

The interferogram is generated by irradiating the sample with infrared light, and the infrared spectrum is obtained by processing the interferogram using the Fourier transform method. Because the absorption peaks of each functional group are different, the functional groups within complex chemical structures can be identified according to the frequency vibration of the absorption peaks [55,56]. The infrared spectrum of three asphaltenes shows that the distribution range of absorption peaks is similar, mainly concentrated in two wave numbers of 700–1700 cm^{-1} and 2700–3300 cm^{-1} (Fig. 10).

The infrared spectrums were integrated after baseline correction and smoothing processing, the results are shown in Table 6. The peaks at 801.19 and 1261.24 cm^{-1} represent N–H bonds and C-N bonds in amine. The peaks related to sulfur are located at 701.51 and 1021.36 cm^{-1}, representing the C-S bond in the aliphatic and the S = O bond in the sulfoxide [29]. The recognition peak of the C-O bond in alcohols appears at 1092.56 cm^{-1}. The C–H bonds in alkanes and the C–C bonds in aromatics appear in the spectral range of 1375.36–1601.18 cm^{-1}. The vibrations of methyl and methylene groups in naphthenes are predominantly observed in the wave number range of 2854.62–2959.12 cm^{-1}. A total of 13 absorption peaks were identified, corresponding to 7 types of functional groups.

The integration results showed that alkane, naphthene, and aliphatic hydrocarbon structures were the most abundant among the three asphaltenes (75.11 %–82.16 %), while the proportion of heteroatoms, hydroxyl, and carboxyl functional groups was relatively small. The proportion of absorption peak areas of LBL, MBL, and HBL in the wave number range of 1021.36–1092.56 cm^{-1} (alcohols and sulfoxides) were 21.91 %, 10.86 %, and 22.57 %, respectively, and showed a trend of decreasing first and then increasing with the increase of biodegradation

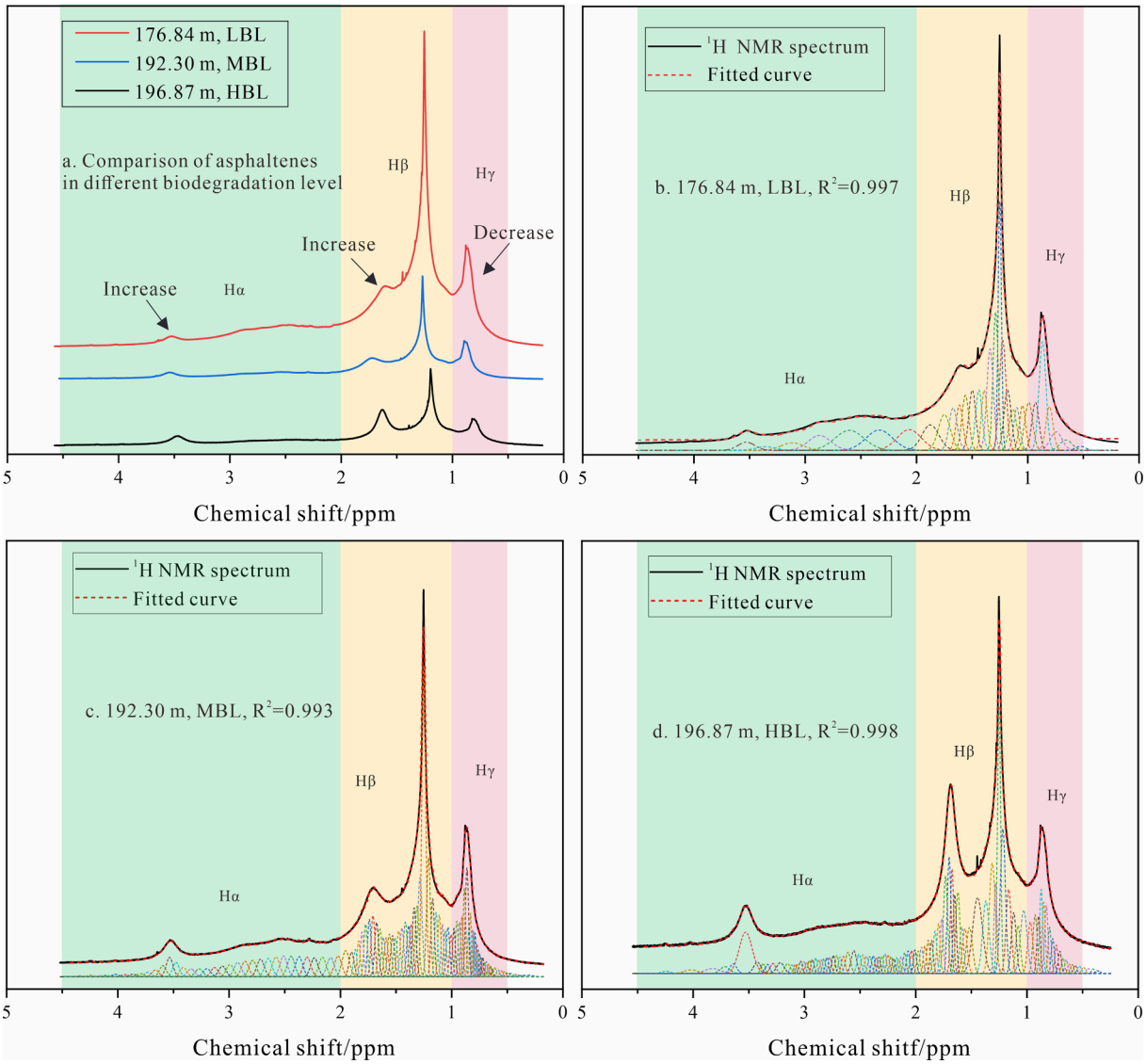

Fig. 9. Peak fitting of nuclear magnetic resonance hydrogen spectroscopy was conducted to compare the differences in the proportions of hydrogen atom types in asphaltenes at varying levels of biodegradation, providing fundamental information about their chemical structures. As the biodegradation level increases, the proportion of H_γ decreases, while the proportion of H_β and H_α increases.

Table 5
The types of hydrogen and their relative peak area proportions in asphaltenes at different levels of biodegradation.

Chemical shift/ppm	symbol	Structural assignment	Relative proportion/%		
			LBL	MBL	HBL
0.1–1.0	H_γ	CH_3 of chain/paraffin hydrocarbons (isolated or terminal), in the γ position	20.27	17.10	14.50
1.0–1.5	$H_{\beta\text{-}2}$	CH_2 of paraffin hydrocarbons in β position or further aromatic rings	43.80	39.61	35.95
1.5–2.0	$H_{\beta\text{-}1}$	CH_2 of paraffinic and naphthenic in β position of aromatic rings	16.10	21.15	25.33
2.0–4.5	$H_{\alpha\text{-}1}$	CH, CH_2, CH_3 of paraffinic and naphthenic hydrocarbons linked on the α position of aromatics	18.00	17.76	17.68
3.4–4.5	$H_{\alpha\text{-}2}$	hydrogens α to two aromatic rings simultaneously	1.76	4.27	6.40
6.0–9.0	H_{ar}	total hydrogen in the aromatics	0.07	0.11	0.14

level. The alcohol, amines, and carbonyl are the priority targets of biodegradation, resulting in the relative proportion of methyl and methylene in the naphthenes of MBL asphaltene increasing significantly. Further biodegradation results in the destruction of methyl and methylene groups in naphthenes, causing the absorption peak in the range of 2700–3300 cm^{-1} to return to the initial state (Fig. 10). The characteristics of HBL asphaltene in the infrared spectrum mainly reflect the further increase of the proportion in the naphthenes and heteroatom-related functional groups, consistent with the experimental results of elemental analysis and ^1H NMR.

4. Discussion

4.1. Construction and aggregation of asphaltene molecular model

In previous studies, the molecular weight of asphaltene is measured by gel chromatography experiments, within a range of several thousand [31,57]. Additionally, our experimental results indicate that the chemical structure of asphaltenes is primarily composed of aliphatic and aromatic components, with a total of approximately 10 to 30 rings. This finding lays the groundwork for constructing the carbon skeletal

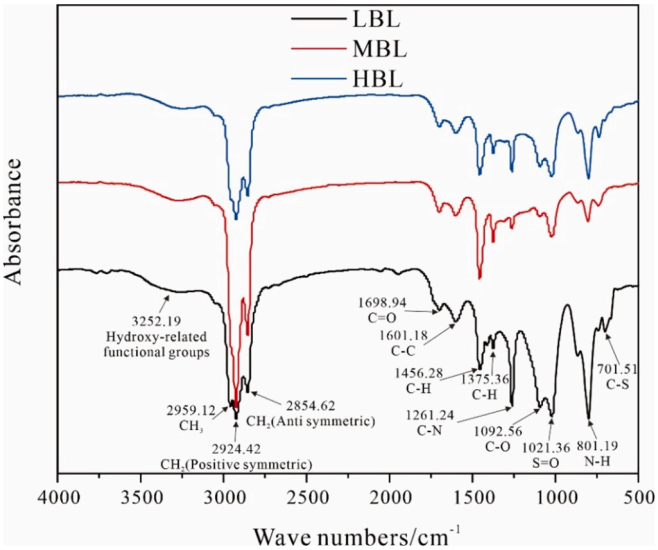

Fig. 10. Fourier transform infrared spectra of the asphaltenes with different biodegradation levels, the proportion of each functional group was calculated quantitatively by integrating. The highest proportions are found in methyl and methylene groups, while the proportions of other nitrogen, oxygen, and sulfur-containing functional groups show considerable variation.

structure of asphaltenes. The relative proportions of carbon, hydrogen, oxygen, nitrogen, and sulfur provide insight into the ratios of different atom types. Finally, modifying the number of branched chains and various functional groups, as well as the degree of oxygen substitution and condensation. The two-dimensional molecular structures of three asphaltenes, LBL, MBL, and HBL, were constructed respectively (Fig. 11), and their molecular formulas are as follows: $C_{94}H_{131}NO_2S_3$, $C_{100}H_{125}NO_3S_3$, and $C_{114}H_{129}NO_5S_4$. The number of atoms is 230, 232, and 253, respectively, and the relative molecular mass is 1371.21, 1483.88, and 1719.88.

It is indeed challenging to precisely quantify the chemical structure of a complex mixture like asphaltene. However, constructing average molecular models enables us to closely match the experimental data. Therefore, the constructed molecular model can effectively represent the actual chemical characteristics of asphaltene, achieving the goal of modeling. On the molecular model scale, the number of atoms per unit and the relative molecular weight increase with the biodegradation level, consistent with previous results [16,24]. The proportion of carbon (82.34 %–79.54 %), hydrogen (9.63 %–7.55 %), nitrogen (0.81 %–1.02 %), oxygen (2.33 %–4.65 %), and sulfur (4.68 %–7.45 %) elements is consistent with the elemental analysis data.

The condensation degree of the asphaltene model ranges from 0.29 to 0.38, the oxygen substitution degree ranges from 0.20 to 0.31, and the branched-chain length parameter ranges from 0.14 to 0.27. In these asphaltene molecular models, sulfur and nitrogen are predominantly carried by aliphatic sulfur, aromatic sulfur, and pyrrole structures. With the increase in biodegradation level, the proportion of hydroxyl, phenolic and ether functional groups decreased, while the proportion of carboxyl and ketone functional groups increased. This trend is consistent with the XPS experimental results, suggesting structural changes due to biodegradation. The average molecular model constructed by this method effectively characterizes the chemical structural differences of asphaltene with different biodegradation levels.

To further verify the reliability of the model, MestReNova software is used to predict the molecular models of three asphaltenes by ^{1}H NMR. The predicted results were fitted with the original hydrogen spectrum data, yielding an average R^2 value of 0.93 (Appendix Fig. S1). However, small differences were observed in the 1–1.5 and 3–4 ppm parts of the spectrum, due to the spatial arrangement of atoms in the two-dimensional structure affecting the prediction results [50,58].

A three-dimensional molecular model of asphaltene is obtained by geometric optimization, annealing, and dynamic simulation of two-dimensional structures under periodic boundary conditions. The asphaltene molecular model is constructed using the aggregation process described by the Yen-Mullins aggregation model (Fig. 12) [37,38]. Due to π-π interactions, the aromatic ring structure between monomer asphaltene molecules forms face-face or edge-face stacked dimers, trimers, or multimers. As concentration increases, the number of asphaltene polymers grows, leading to the formation of clusters at high concentrations [37,38,59]. The optimized three-dimensional asphaltene model was constructed as a parallel dimers structure, achieved through the conjugate gradient optimization method was used to obtain the lowest energy molecular configuration. The amorphous cell calculation module in the material studio software is combined to form a nano-aggregate containing 4–5 asphaltene molecules (Fig. 12 red part). The range of relative molecular weight of the asphaltene nanoaggregates constructed by this method is 5000–6000, which is consistent with the previously reported experimental data [30,31,57].

4.2. Assembly and verification of bitumen molecular model

For the complex chemical composition of bitumen, the four-component (includes asphaltene, resin, saturated and aromatic hydrocarbons) method is highly effective according to the different polarities [60]. The fractions of saturated and aromatic hydrocarbon are determined based on the GC–MS results, and the asphaltene fractions are represented by the asphaltene nanoaggregate molecular model constructed above, while the resin fraction refers to the molecular model reported previously ($C_{60}H_{87}NOS$) [31]. To construct a four-component bitumen molecular model, the experimental results of elemental analysis and fraction separation were used as constraint conditions. This approach ensures that the model accurately represents the actual

Table 6
The integration results of the infrared spectra for asphaltenes at different levels of biodegradation indicate that alcohol and sulfoxide structures are consumed preferentially.

Number	Wave numbers/cm^{-1}	Corresponding functional groups	LBL/%		MBL/%		HBL/%	
1	701.51	C-S bond in aliphatic	2.65	2.65	2.60	2.60	1.63	1.63
2	801.19	N–H bond in amines	10.48	10.48	3.37	3.37	8.83	8.83
3	1021.36	S = O bond in sulfoxide	6.53	21.91	7.44	10.86	12.61	22.57
4	1092.56	C-O bond in alcohol	15.38		3.42		9.96	
5	1261.24	C-N bond in aromatic amines	9.91	26.86	2.97	22.81	7.41	30.06
6	1375.36	C–H bond rock in alkane	4.44		4.74		5.10	
7	1456.28	C–H bond bend or scissoring in alkane	6.53		9.99		10.38	
8	1601.18	C–C bond stretch (in ring) in aromatic	5.98		5.11		7.16	
9	1698.94	C = O bond in carbonyl	3.50	3.50	3.38	3.38	4.20	4.20
10	2854.62	Anti-symmetric vibration of naphthenes or aliphatic methylides	8.05	26.34	14.18	46.83	10.79	29.53
11	2924.42	Positive-symmetric vibration of naphthenes or aliphatic methylides	8.83		21.86		13.48	
12	2959.12	Vibrations of methyl groups in naphthenes or aliphatic groups	9.46		10.79		5.25	
13	3252.19	Hydroxy-related (phenol hydroxyl, hydrogen bond, alcohol hydroxyl)	8.26	8.26	10.15	10.15	3.18	3.18

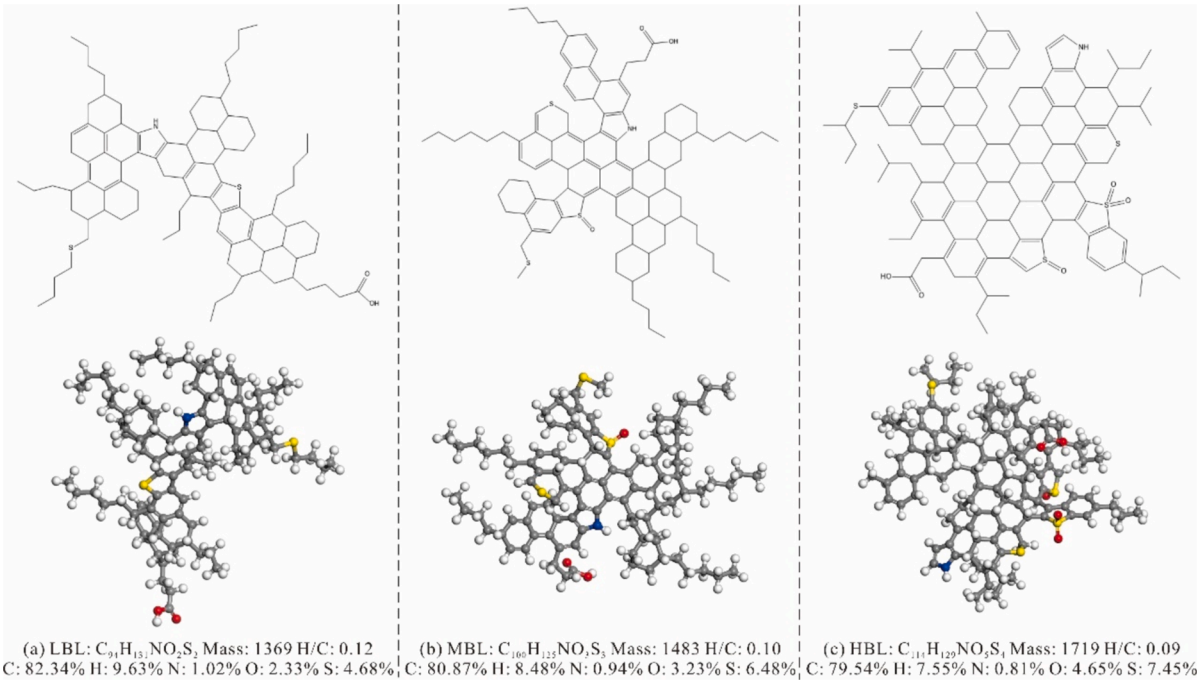

Fig. 11. Two-dimensional molecular structures of the three asphaltenes were constructed and optimized, forming three-dimensional molecular models. The biodegradation levels from low to high are LBL (C_{94} H_{131} NO_2 S_2), MBL (C_{100} H_{125} NO_3 S_3), and HBL (C_{114} H_{129} NO_5 S_4). Molecular weight, element proportion, fraction of aromatic carbon, degree of condensation and oxygen substitution, and branch chain length are consistent with the experimental results.

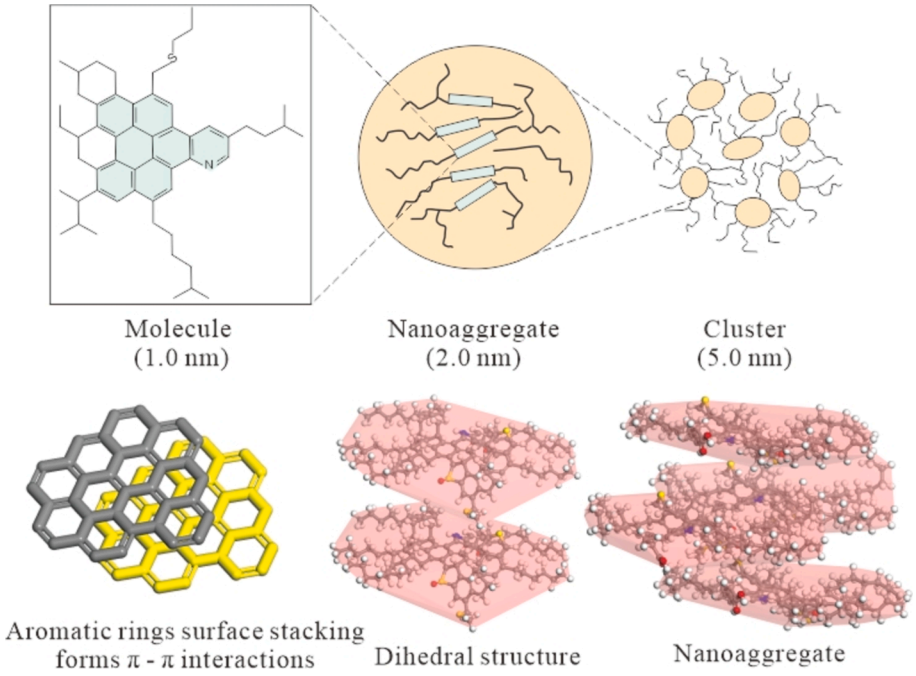

Fig. 12. The asphaltene nanoaggregates model was constructed based on the Yen-Mullins asphaltene aggregation model [37,38], the π-π interactions between the aromatic rings of monomer asphaltene molecules lead to the formation of the dimers, and multiple dimers stack to form asphaltene nanoaggregates.

chemical composition and distribution of the different components within bitumen.

To ensure both representativeness and sensitivity to biodegradation, it is crucial to select compounds that are relatively abundant and show significant changes with biodegradation levels [24,25]. For the saturated hydrocarbon fraction, three typical compounds were selected: C_{23}TT ($C_{23}H_{42}$), C_{30}H ($C_{30}H_{52}$) and C_{21} pregnane ($C_{21}H_{36}$). Similarly, the compounds with no fewer than three aromatic rings of 1, 2, 6-TMP ($C_{17}H_{16}$), 3-MChy ($C_{19}H_{14}$), and C_{28} TAS 20R ($C_{28}H_{34}$) were selected as representative of aromatic hydrocarbons fraction. Based on the asphaltene nanoaggregates as the core, the molecules quantities of the resin, saturated, and aromatic hydrocarbon fractions were continuously adjusted to match with the experimental data on the relative proportions of each component (Fig. 13).

A comprehensive comparison of the experimental data and molecular model data is presented in Table 7, these models accurately

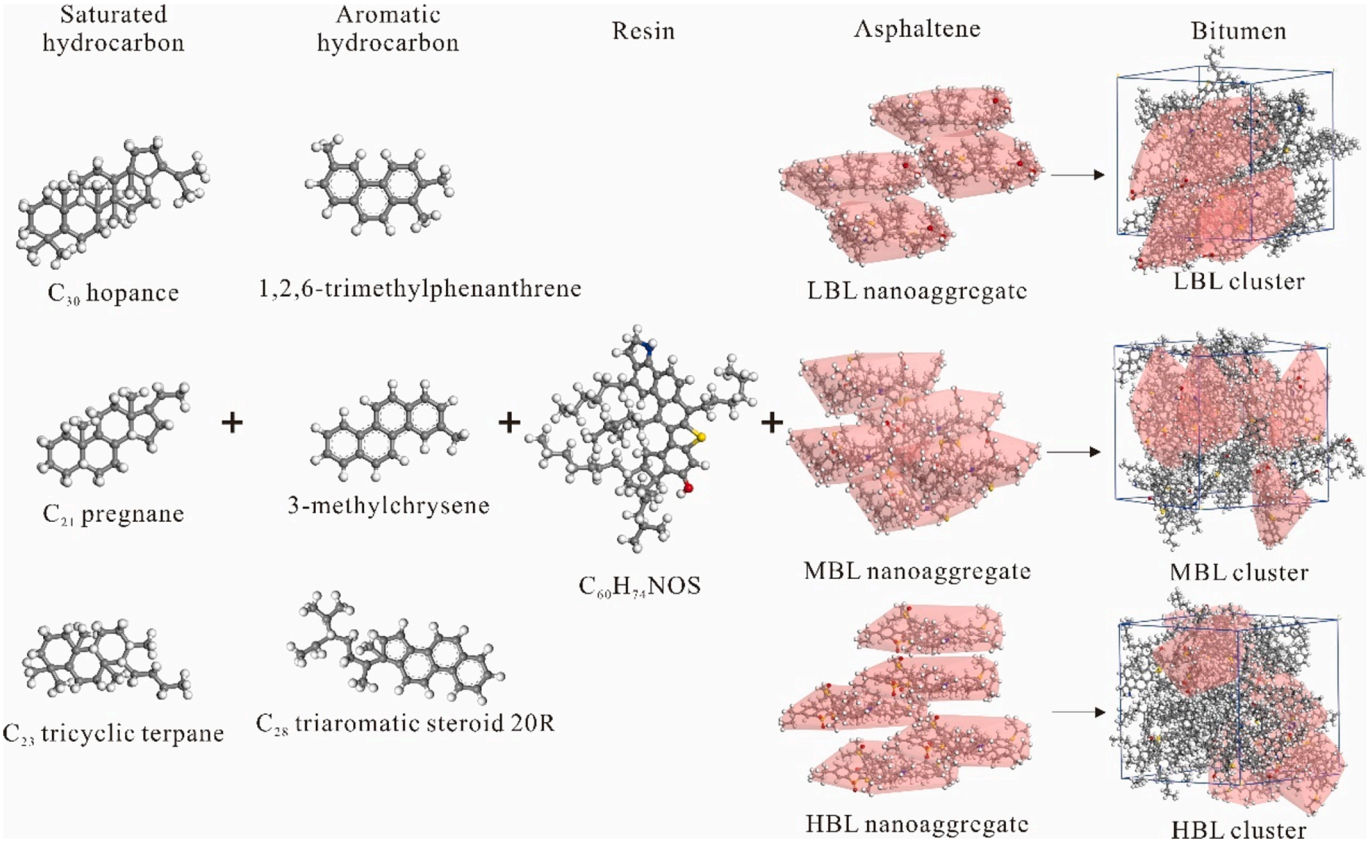

Fig. 13. Construction method of four-component bitumen cluster molecular models. Saturated hydrocarbons are characterized by C_{21} pregnane, C_{23} tricyclic terpane, and C_{30} hopane, while 1,2,6-trimethylphenanthrene, 3-methylchrysene, and C_{28} triaromatic steroids 20R represent aromatic. Macromolecular compounds containing nitrogen, oxygen, and sulfur represent resins and asphaltenes. Resins surround the asphaltene nanoaggregate, while saturated and aromatic hydrocarbon molecules are dispersed as the continuous phase within the system.

Table 7
The proportions of each component in the bitumen molecular model were compared with experimental results, with all errors not exceeding 1%, thereby validating the accuracy of the molecular model.

Sample	Four compositions	Compound type	Experimental proportion/ %	Experimental total/ %	Molecules number	Model proportion/ %	Model total/ %	Error/ %
LBL	Sat	$C_{30}H$	15.19	24.47	7	15.10	24.50	−0.09
		$C_{23}TT$	6.50		4	6.50		0.00
		C_{21}pregnane	2.78		2	2.90		0.12
	Aro	1, 2, 6-TMP	4.02	30.65	3	3.57	30.37	−0.45
		3-MChy	5.10		4	4.90		−0.20
		C_{28} TAS 20R	21.53		12	21.90		0.37
	Res	$C_{60}H_{87}NOS$	18.17	44.88	4	18.10	45.13	−0.07
	Asp	$C_{94}H_{131}NO_2S_2$	26.71		4	27.03		0.32
MBL	Sat	$C_{30}H$	13.06	22.51	8	13.70	22.90	0.64
		$C_{23}TT$	7.28		5	6.60		−0.68
		C_{21}pregnane	2.17		2	2.60		0.43
	Aro	1, 2, 6-TMP	2.89	20.88	3	2.80	20.70	−0.09
		3-MChy	4.23		4	4.00		−0.23
		C_{28} TAS 20R	13.76		9	13.90		0.14
	Res	$C_{60}H_{87}NOS$	24.67	56.61	7	25.40	56.40	0.73
	Asp	$C_{100}H_{125}NO_3S_3$	31.94		5	31.00		−0.94
HBL	Sat	$C_{30}H$	7.60	18.05	4	6.70	16.70	−0.90
		$C_{23}TT$	7.87		6	7.70		−0.17
		C_{21}pregnane	2.58		2	2.30		−0.28
	Aro	1, 2, 6-TMP	3.12	23.46	4	3.60	24.00	0.48
		3-MChy	3.73		4	3.90		0.17
		C_{28} TAS 20R	16.61		11	16.50		−0.11
	Res	$C_{60}H_{87}NOS$	24.76	58.49	7	24.60	59.30	−0.16
	Asp	$C_{114}H_{129}NO_5S_4$	33.73		5	34.70		0.97

Sat: saturate; Aro: aromatic; Res: resin; Asp: asphaltene; C_{30} H: C_{30} hopane; C_{23} TT: C_{23} tricyclic terpanes; TMP: trimethylphenanthrene; 3-MChy: 3-methylchrysene; C_{28} TAS 20R: C_{28} triaromatic steroids 20R;

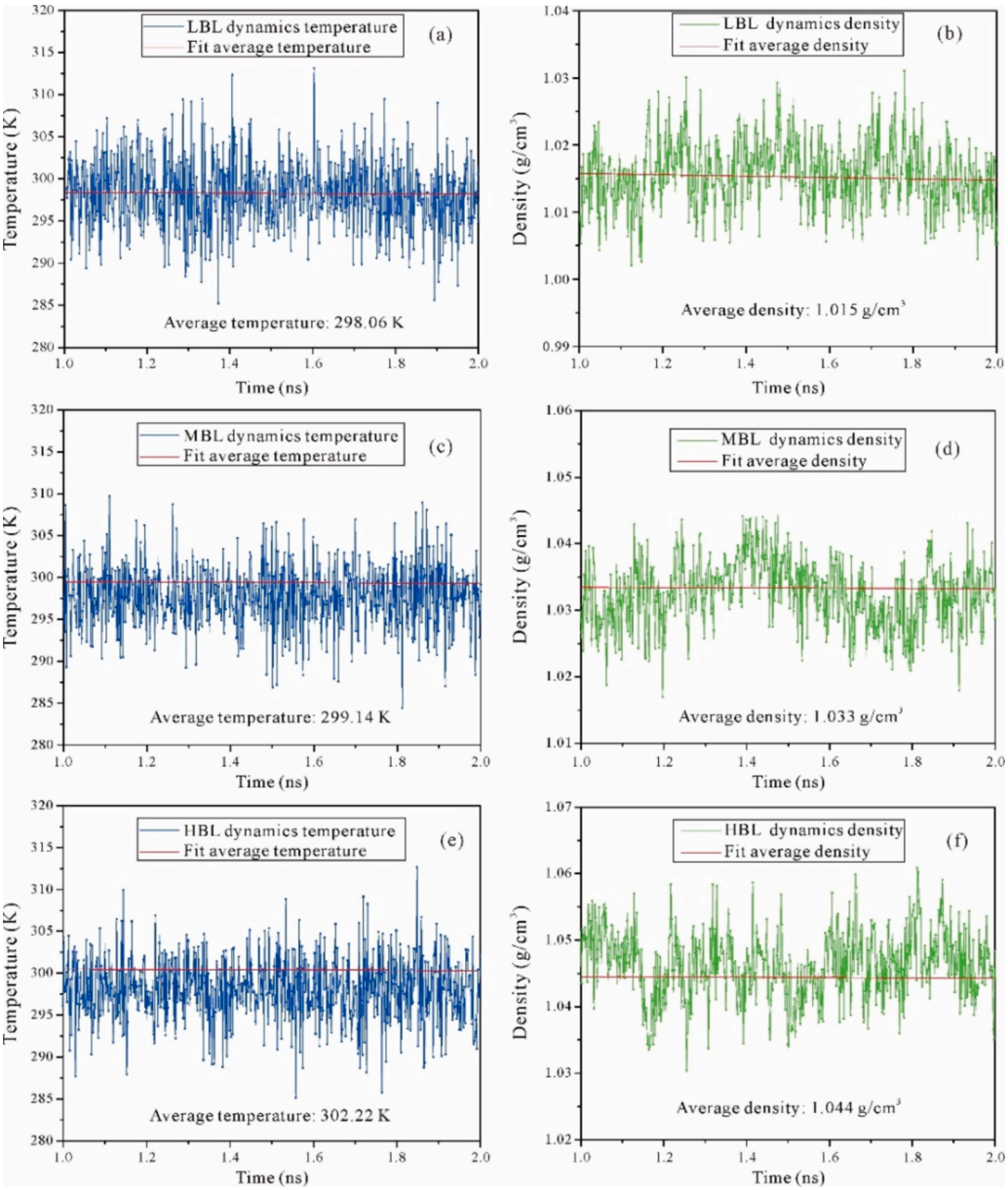

Fig. 14. In the NPT ensemble (at 298 K and 0.1 MPa), the dynamic equilibrium process of the bitumen molecular model was observed, with temperature and density reaching equilibrium after 1 ns. The density obtained from molecular dynamics simulations aligns with experimental values, thereby validating the reliability of the model.

represent the mass proportion of the compounds, with an error of less than 1 %. Due to the relatively low biodegradation level of LBL bitumen, the mass proportions of saturated and aromatics hydrocarbons are higher (54.87 %, 32 molecules), while the mass proportions of resin and asphaltenes are lower (45.13 %, 8 molecules). The compounds $C_{30}H$ and C_{28} TAS 20R in the LBL bitumen model have the highest mass proportions among all the bitumen models.

The MBL and HBL bitumen have relatively high biodegradation levels, with both employing five asphaltene molecules as nano-aggregates, the mass proportions of asphaltenes add resins are 56.4 % and 59.3 %, respectively. In the MBL bitumen model, the mass proportions of saturated hydrocarbons (22.9 %) and aromatic (20.7 %) components are relatively balanced. As HBL bitumen exhibit the highest level of biodegradation among the three samples, the mass proportion of saturated hydrocarbons (16.7 %) further decreases relative to aromatics (24.0 %). The number of $C_{30}H$ molecules (4 molecules) is the lowest among all the bitumen models, which is consistent with the earlier GC–MS experimental results.

Geometric optimization, annealing treatment, and dynamic simulation were carried out to obtain the basic physical property of these bitumen molecular models in the equilibrium state. During the simulation, the initial and final temperatures of the three bitumen models showed no significant fluctuations, and the energy changes were minimal, indicating that the system had reached an equilibrium state (Fig. 14a, c, e). In addition, density, as an important parameter, was also included in the verification of whether the model is reasonable [41,61]. Simulations were performed under normal temperature (298.15 K) and pressure (1 atm) with the NPT ensemble. The simulation reached the equilibrium state after 1 ns, and the densities of the LBL MBL and HBL bitumen molecular models at normal temperature and pressure were 1.015 g/cm^3, 1.033 g/cm^3 and 1.044 g/cm^3 respectively (Fig. 14b, d, f), which are very close to the experimentally measured values of 1.005 g/cm^3 and 1.012 g/cm^3 at the same conditions [62,63]. The simulated values for MBL and HBL bitumen were slightly higher than the measured

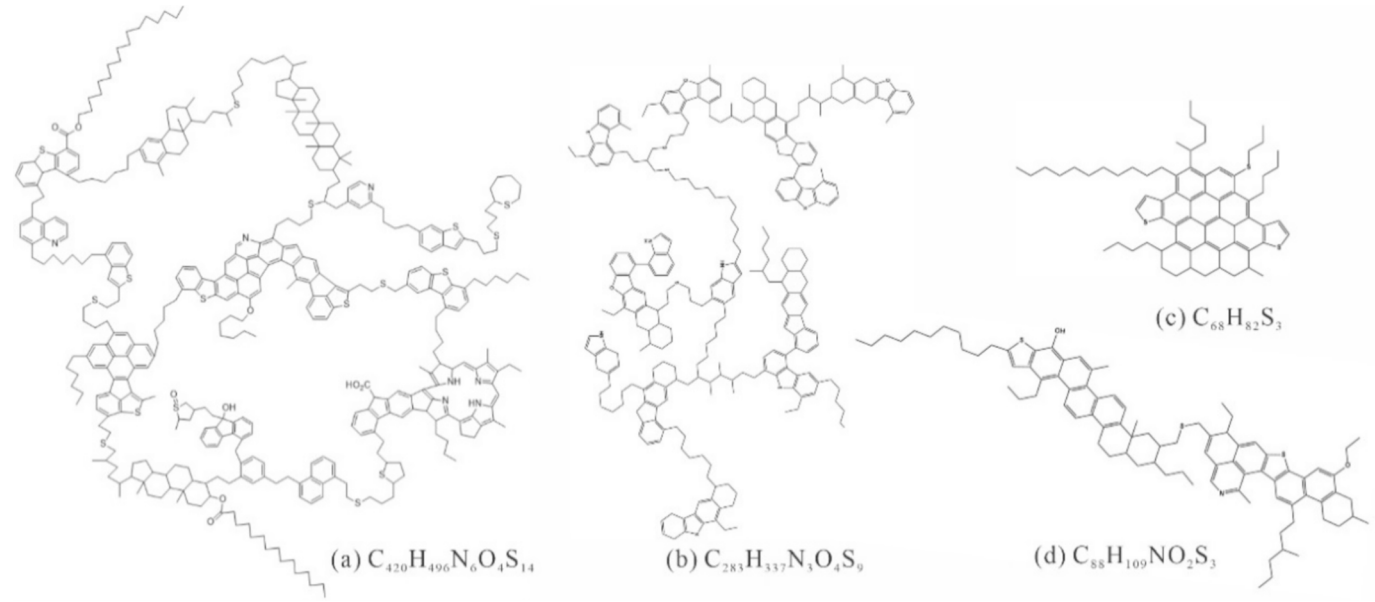

Fig. 15. The understanding of the asphaltene molecular structure has shifted from the archipelagic model (a, b) [35,36] to the island model (c, d) [31,33]. Currently, the island model of asphaltene is widely accepted. However, the Athabasca asphaltene island model (c, d) proposed in previous reports lacks comprehensive characterization of heteroatom types and functional groups. The model developed in this study incorporates additional details for improved accuracy.

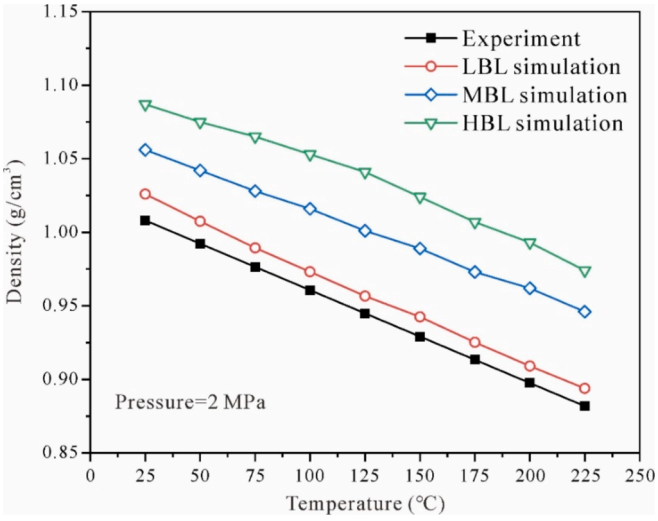

Fig. 16. Molecular dynamics simulations were used to predict the variation of bitumen density with temperature at 2 MPa. The results indicate that bitumen density is negatively correlated with temperature, and the trend in density variation for the lower biodegradation level LBL bitumen aligns with experimental values [71]. Simulations can further enhance our understanding of the various physical and chemical properties of bitumen.

values, which may be attributed to the use of bitumen samples with a lower level of biodegradation in the laboratory.

The density value of the bitumen molecular models shows a positive correlation with the biodegradation level, which is consistent with previous studies and further validates the practical significance of the molecular models [16]. Furthermore, during the simulation process, the resin, saturated and aromatic hydrocarbon gradually converge toward the asphaltene aggregate molecules. The distribution of different component molecules within the system is not uniform; rather, they are constrained in clusters, forming a relatively stable state. This observation aligns with results previously reported through atomic force microscopy [55,64].

4.3. Advantages and application prospect

The understanding of asphaltene structure has evolved from the macromolecules (archipelago model) in the early 1990 s to the fact that asphaltene is composed of relatively small polycyclic aromatic hydrocarbons (island model). The molecular model of Athabasca archipelagic asphaltenes was established in the research's early stages, through the vapor pressure osmometry (VPO) method (Fig. 15a, b) [35,36], while Bruno et al. proposed different opinions in their 2020 report [65]. Despite the controversy, increasing experimental evidence supports the view that asphaltene is composed of smaller, isolated molecules. For instance, fluorescence depolarization (FD) technology results indicate that the average molecular weight of petroleum asphaltene is approximately 750 amu, suggesting relatively small asphaltene molecules [66]. Observations using atomic force microscopy have revealed the absence of large molecules in the asphaltene microstructure. Additionally, asphaltene fragments obtained via laser desorption laser ionization mass spectrometry show that compounds with a single aromatic core structure remain unfragmented, providing evidence supporting the island model of asphaltene structure [67]. However, studies on the Athabasca asphaltene island model have faced challenges, including the relatively small molecular weight, limited types of heteroatom, and incomplete characterization of functional groups (Fig. 15c, d) [31,33]. Furthermore, characterizing complex hydrocarbon mixtures such as heavy oil or bitumen through single-molecule models has a significant drawback: the inability to accurately understand the thermodynamic behavior of individual fractions within the cluster system [41,53,61].

Overall, different analysis methods and perspectives may lead to multiple models, and selecting the most suitable model based on research objectives is conducive to improving the accuracy of simulation results. The molecular model constructed in this study has the following advantages: Firstly, many previous reports have analyzed the impact of organic matter sources and maturity on chemical structure [68,69]. However, there remains controversy over whether the chemical structure of asphaltene will be affected by biodegradation. In this research, all samples were from one oil column, excluding the influence of organic matter sources, sedimentary environment, and maturity. The primary focus of this study was on the effect of severe biodegradation on the chemical composition of bitumen. Additionally, the molecular models

comprising the saturated and aromatic hydrocarbon fractions were rigorously determined using GC–MS experiments. The Yen-Mullins model of asphaltene aggregation guided the construction of asphaltene nanoaggregates, with saturated and aromatic hydrocarbon molecular dispersed as a continuous phase in the system, forming the molecular models of bitumen cluster [37].

The complexity and diversity of bitumen's chemical components make it challenging to measure and observe under laboratory conditions. With advancements in computational science and computer performance, molecular dynamics simulations have become crucial for deeper understanding and predictive modeling of molecular systems in heavy oil and bitumen [40,70]. These simulations help describe the microscopic properties that are otherwise difficult to measure in the laboratory, making them increasingly important in the petroleum industry.

The bitumen in the oil sands is heated by injecting water vapor into the reservoir. The high temperature causes a decrease in bitumen density and viscosity, increasing its fluidity, which benefits recovery [2,13]. Temperature's influence on the bitumen properties is crucial, but acquiring related laboratory data is costly. Molecular dynamics simulations can predict how bitumen properties change under various temperatures and pressures. Under a constant pressure of 2 MPa and a temperature ranging from 25 to 225℃ (water vapor temperature), experimental and simulated values of bitumen density exhibit consistent trends (Fig. 16) [71]. LBL bitumen, with relatively low biodegradation levels, has a lower density than water after heating to 100℃, while MBL and HBL bitumen, with higher biodegradation levels, may require temperatures exceeding 150℃.

Through this process, the physical properties of diverse complex hydrocarbons, their microscopic thermodynamic behavior with inorganic minerals, and interactions among each component can be accurately and cost-effectively predicted. This offers a more optimized strategy for development, reducing costs and better meeting the current requirements for enhancing heavy oil and oil sand recovery efficiency.

5. Conclusion

To enhance understanding of the heterogeneity of fluids in heavy oil and oil sands reservoirs, this study analyzes the chemical composition of bitumen with varying biodegradation levels within oil column from the MacKay River area and develops three novel molecular models. Due to significant biodegradation (PM 5–6), most saturated and aromatic hydrocarbons were largely depleted, while more resistant compounds, such as terpanes and polycyclic aromatic hydrocarbons (with three or more rings), became predominant. Furthermore, asphaltenes at different biodegradation levels exhibited variations in molecular structure, elemental ratios and functional groups.

Based on experimental data, three molecular models representing bitumen clusters (four-components) at different biodegradation levels were constructed. The Yen-Mullins asphaltene aggregation model was utilized to ensure the molecular models aligned with actual observations. The dynamic simulation results for asphaltene density corresponded closely with measured values, confirming the reliability of the findings. This study enhances the understanding of the chemical composition of bitumen at various biodegradation levels and provides a rapid, low-cost method for predicting bitumen physical properties, which can assist in optimizing development strategies during production processes.

CRediT authorship contribution statement

Junhao Ren: Writing – review & editing, Writing – original draft, Software, Methodology. **Ningning Zhong:** Supervision. **Meijun Li:** Supervision, Project administration. **Xiaofa Yang:** Resources. **Sibo Yang:** Validation. **Bang Zeng:** Formal analysis. **Xiaoqiang Liu:** Visualization, Validation.

Declaration of competing interest

The authors declare that they have no known competing financial interests or personal relationships that could have appeared to influence the work reported in this paper.

Acknowledgments

This work was funded by the National Natural Science Foundation of China (42472177). We thank the Alberta Energy Regulator and BRION Energy corporation for their support with the oil sand samples and basic information. We extend our gratitude to the Guangzhou Institute of Geochemistry, Chinese Academy of Sciences, and the Research Institute of Petroleum Exploration and Development for their invaluable support and cooperation in this research. We thank the National Key Laboratory of Petroleum Resources and Engineering, China University of Petroleum (Beijing) for providing experimental technology and equipment. Special thanks are due to laboratory staff, Shengbao Shi and Lei Zhu, for their assistance in ensuring the smooth progress of the experimental analysis. Finally, we sincerely thank the editor and reviewers for their valuable suggestions on this manuscript.

Appendix A. Supplementary data

Supplementary data to this article can be found online at https://doi.org/10.1016/j.fuel.2024.134248.

Data availability

Data will be made available on request.

References

[1] Alberta Energy Regulator. Alberta's energy reserves 2013 and supply/demand outlook 2014-2023. Alberta's Energy Reserves 2013 and Supply/Demand Outlook. Calgary, AB, Canada; 2014.
[2] Schiltz K, Gray D. Monitoring and Predicting Steam Chamber Development in a Bitumen Field. Unconventional Oil and Gas Resources Handbook. Waltham, MA: Gulf Professional Publishing; 2016. p. 495–512.
[3] Rahnama F, Marsh RA, Philp L. The Alberta oil sands: Reserves and long-term supply outlook. AAPG Stud Geol 2013;64:133–44.
[4] Martinius A, Fustic M, Garner D, Jablonski B, Strobl R, MacEachern J, et al. Reservoir characterization and multiscale heterogeneity modeling of inclined heterolithic strata for bitumen-production forecasting, McMurray Formation, Corner, Alberta. Canada Marine and Petroleum Geology 2017;82:336–61.
[5] Yang X, Yu D, Wu S, Ren J, Cheng D, Huang J, et al. Impact of Reservoir Heterogeneity on Bitumen Content in Mackay River Oil Sands, Athabasca (Canada). Acta Geologica Sinica-English Edition 2024;98(5):1285–300.
[6] Mossop GD. Geology of the Athabasca Oil Sands. Science 1980;207(4427):145–52.
[7] Bennett B, Adams J, Gray N, Sherry A, Oldenburg T, Huang H, et al. The controls on the composition of biodegraded oils in the deep subsurface–Part 3. The impact of microorganism distribution on petroleum geochemical gradients in biodegraded petroleum reservoirs. Org Geochem 2013;56:94–105.
[8] Ren J, Li M, Yang X, Yang C, Ma G, Huang J, et al. Effects of matrix on oil sands texture and bitumen distribution in the Cretaceous McMurray Formation, Alberta. Canada Geoenergy Science and Engineering 2024;237:212807.
[9] Day-Stirrat RJ, Hillier S, Nikitin A, Hofmann R, Mahood R, Mertens G. Natural gamma-ray spectroscopy (NGS) as a proxy for the distribution of clay minerals and bitumen in the Cretaceous McMurray Formation, Alberta. Canada Fuel 2021;288:119513.
[10] Abram M, Cain G. Particle-Size Analysis for the Pike 1 Project, McMurray Formation. J Can Pet Technol 2014;53(06):339–54.
[11] Fustic M, Strobl R, Fowler M, Jablonski BV, Martinius AW. Impact of reservoir heterogeneity on oil migration and the origin of oil-water contacts: McMurray Formation type section, Alberta. Canada Marine and Petroleum Geology 2019;103:216–30.
[12] Fustic M, Bennett B, Hubbard SM, Huang H, Oldenburg T, Larter S. Impact of reservoir heterogeneity and geohistory on the variability of bitumen properties and on the distribution of gas-and water-saturated zones in the Athabasca oil sands, Canada, Heavy-oil and oil-sand petroleum systems in Alberta and beyond. AAPG Stud Geol 2013;64:163–205.
[13] Larter S, Adams J, Gates I, Bennett B, Huang H. The origin, prediction and impact of oil viscosity heterogeneity on the production characteristics of tar sand and heavy oil reservoirs. J Can Pet Technol 2008;47(01).
[14] Adams J, Larter S, Bennett B, Huang H, Kruisdijk CV. The dynamic interplay of oil mixing, charge timing, and biodegradation in forming the Alberta oil sands:

Insights from geologic modeling and biogeochemistry. AAPG Stud Geol 2013;64:23–102.
[15] Hwang R, Ahmed A, Moldowan J. Oil composition variation and reservoir continuity: Unity field. Sudan Organic Geochemistry 1994;21(2):171–88.
[16] Connan J. Biodegradation of crude oils in reservoirs. Lodon: Academic Press; 1984.
[17] Larter S, Head I, Huang H, Bennett B, Jones M, Aplin A, et al. Biodegradation, gas destruction and methane generation in deep subsurface petroleum reservoirs: an overview. In: Society G, editor. Petroleum Geology Conference series. London: The Geological Society of London; 2005. p. 633–9.
[18] Head IM, Jones DM, Larter SR. Biological activity in the deep subsurface and the origin of heavy oil. Nature 2003;426(6964):344–52.
[19] Hein FJ. Heavy Oil and Oil (Tar) Sands in North America: An Overview & Summary of Contributions. Nat Resour Res 2006;15(2):67–84.
[20] Hein FJ. Geology of bitumen and heavy oil: An overview. J Pet Sci Eng 2017;154:551–63.
[21] Larter S, Wilhelms A, Head I, Koopmans M, Telnaes N. The controls on the composition of biodegraded oils in the deep subsurface—part 1: biodegradation rates in petroleum reservoirs. Org Geochem 2003;34(4):601–13.
[22] Larter S, Huang H, Adams J, Bennett B, Jokanola O, Oldenburg T, et al. The controls on the composition of biodegraded oils in the deep subsurface: Part II—Geological controls on subsurface biodegradation fluxes and constraints on reservoir-fluid property prediction. AAPG Bull 2006;90(6):921–38.
[23] Oldenburg TB, Jones M, Huang H, Bennett B, Shafiee NS, Head I, et al. The controls on the composition of biodegraded oils in the deep subsurface–Part 4. Destruction and production of high molecular weight non-hydrocarbon species and destruction of aromatic hydrocarbons during progressive in-reservoir biodegradation. Org Geochem 2017;114:57–80.
[24] Peters KE, Walters CC, Moldowan JM. The Biomarker Guide: Biomarkers and Isotopes in Petroleum Exploration and Earth History. secend ed. Cambridge: Cambridge University Press; 2005.
[25] Peters KE, Moldowan JM. The Biomarker Guide: interpreting Molecular Fossils in Petroleum and Ancient Sediments. Englewood Cliffs, New Jersey: Prentice Hall; 1993.
[26] Bennett B, Larter S. Biodegradation scales: Applications and limitations. Org Geochem 2008;39(8):1222–8.
[27] Larter S, Huang H, Adams J, Bennett B, Snowdon LR. A practical biodegradation scale for use in reservoir geochemical studies of biodegraded oils. Org Geochem 2012;45(2):66–76.
[28] Zuo JY, Jackson R, Agarwal A, Herold B, Kumar S, Santo ID, et al. Diffusion model coupled with the Flory–Huggins–Zuo equation of state and Yen–Mullins model accounts for large viscosity and asphaltene variations in a reservoir undergoing active biodegradation. Energy Fuel 2015;29(3):1447–60.
[29] Nagy B, Gagnon GC. The geochemistry of the Athabasca petroleum deposit. I. Elution and spectroscopic analysis of the petroleum from the vicinity of McMurray. Alberta Geochimica et Cosmochimica Acta 1961;23(3–4):155–85.
[30] Speight J. A structural investigation of the constituents of Athabasca bitumen by proton magnetic resonance spectroscopy. Fuel 1970;49(1):76–90.
[31] Suzuki T, Itoh M, Takegami Y, Watanabe Y. Chemical structure of tar-sand bitumens by ^{13}C and ^{1}H n.m.r spectroscopic methods. Fuel 1982;61(5):402–10.
[32] Murgich J, Strausz OP. Molecular mechanics of aggregates of asphaltenes and resins of the Athabasca oil. Pet Sci Technol 2001;19(1–2):231–43.
[33] Murgich J, Rodríguez AY. Molecular recognition and molecular mechanics of micelles of some model asphaltenes and resins. Energy Fuel 1996;10(1):68–76.
[34] Murgich J, Abanero JA, Strausz OP. Molecular recognition in aggregates formed by asphaltene and resin molecules from the Athabasca oil sand. Energy Fuel 1999;13(2):278–86.
[35] Strausz OP, Mojelsky TW, Lown EM. The molecular structure of asphaltene: an unfolding story. Fuel 1992;71(12):1355–63.
[36] Sheremata JM, Gray MR, Dettman HD, McCaffrey WC. Quantitative molecular representation and sequential optimization of Athabasca asphaltenes. Energy Fuel 2004;18(5):1377–84.
[37] Mullins OC. The modified Yen model. Energy Fuel 2010;24(4):2179–207.
[38] Mullins OC, Sabbah H, Eyssautier J, Pomerantz AE, Barré L, Andrews AB, et al. Advances in asphaltene science and the Yen–Mullins model. Energy Fuel 2012;26(7):3986–4003.
[39] Frigerio F, Molinari D. A multiscale approach to the simulation of asphaltenes. Comput Theor Chem 2011;975(1–3):76–82.
[40] Tazikeh S, Shafiei A, Yerkenov T, Abenov A, Seitmaganbetov N, Atabaev TS. A systematic and critical review of asphaltene adsorption from macroscopic to microscopic scale: Theoretical, experimental, statistical, intelligent, and molecular dynamics simulation approaches. Fuel 2022;329:125379.
[41] Ren S, Liu X, Lin P, Gao Y, Erkens S. Molecular dynamics simulation on bulk bitumen systems and its potential connections to macroscale performance: Review and discussion. Fuel 2022;328:125382.
[42] Broughton PL. Devonian salt dissolution-collapse breccias flooring the Cretaceous Athabasca oil sands deposit and development of lower McMurray Formation sinkholes, northern Alberta Basin. Western Canada Sedimentary Geology 2013;283:57–82.
[43] Hein FJ, Fairgrieve B, Dolby G. A Regional Geologic Framework for the Athabasca Oil Sands, Northeastern Alberta. Canada AAPG Stud Geol 2013;64:207–50.
[44] Xiao H, Li M, Wang T, You B, Lu X, Wang X. Organic molecular evidence in the~1.40 Ga Xiamaling Formation black shales in North China Craton for biological diversity and paleoenvironment of mid-Proterozoic ocean. Precambrian Research 2022;381:106848.
[45] Xiao H, Li M, Wang T, You B, Leng J, Han Q, et al. Four series of rearranged hopanes in the Mesoproterozoic sediments. Chem Geol 2021;573:120210.
[46] Chinelatto Júnior LS, Cabral de Menezes SM, HldA H, de Oliveira MCK, Marques LCC. Diffusion-ordered spectroscopy nuclear magnetic resonance as an alternative technique to improve asphaltene characterization. Energy Fuel 2018;32(3):2793–800.
[47] Guzmán HJ, Isquierdo F, Carbognani L, Vitale G, Scott CE, Pereira-Almao P. X-ray photoelectron spectroscopy analysis of hydrotreated athabasca asphaltenes. Energy Fuel 2017;31(10):10706–17.
[48] Liu X-Q, Li M, Zhang C, Fang R, Zhong N, Xue Y, et al. Mechanistic insight into the optimal recovery efficiency of CBM in sub-bituminous coal through molecular simulation. Fuel 2020;266:117137.
[49] Sun H, Ren P, Fried J. The COMPASS force field: parameterization and validation for phosphazenes. Comput Theor Polym Sci 1998;8(1–2):229–46.
[50] Guo C, Li M, Liu X, Xiao H, Luo Q, Han Q, et al. Construction of multidimensional structure model of the Mesoproterozoic Xiamaling shale kerogen, northern North China. Fuel 2024;367:131572.
[51] Huang L, Ning Z, Wang Q, Ye H, Wang Z, Sun Z, et al. Microstructure and adsorption properties of organic matter in Chinese Cambrian gas shale: Experimental characterization, molecular modeling and molecular simulation. Int J Coal Geol 2018;198:14–28.
[52] Ok S, Mal TK. NMR spectroscopy analysis of asphaltenes. Energy Fuel 2019;33(11):10391–414.
[53] Wang Z, Wang Q, Pan S, Jia C, Bai J, Cui D. The chemical structure and thermal evolution of oil Sands bitumen: Experimental and molecular simulation study. J Anal Appl Pyrol 2021;158:105271.
[54] Qing W, Chunxia J, Jianxin G, Wenxue G. ^{1}H NMR and ^{13}C NMR studies of oil from pyrolysis of Indonesian oil sands. Energy Fuel 2016;30(3):2478–91.
[55] He L, Li X, Wu G, Lin F, Sui H. Distribution of saturates, aromatics, resins, and asphaltenes fractions in the bituminous layer of athabasca oil sands. Energy Fuel 2013;27(8):4677–83.
[56] Yolchuyeva UJ, Abbasov VM, Jafarova R, Mammadov A, Ahmadbayova S, Rahimov RA, et al. Chemical composition and molecular structure of asphaltene in Azerbaijani crude oil: A case study of the Zagli field. Fuel 2024;373:132084.
[57] Peramanu S, Pruden BB, Rahimi P. Molecular weight and specific gravity distributions for Athabasca and Cold Lake bitumens and their saturate, aromatic, resin, and asphaltene fractions. Ind Eng Chem Res 1999;38(8):3121–30.
[58] Guan X-H, Liu Y, Wang D, Wang Q, Chi M-S, Liu S, et al. Three-dimensional structure of a huadian oil shale kerogen model: An experimental and theoretical study. Energy Fuel 2015;29(7):4122–36.
[59] Gerken M, Hazendonk P. Solid-State ^{1}H and ^{13}C Nuclear Magnetic Resonance Spectroscopy of Athabasca Oil Sands Asphaltenes: Evidence for Interlocking π-Stacked Nanoaggregates with Intercalated Alkyl Side. Chains 2015.
[60] Hansen JS, Lemarchand CA, Nielsen E, Dyre JC, Schrøder T. Four-component united-atom model of bitumen. J Chem Phys 2013;138(9).
[61] Yao H, Liu J, Xu M, Ji J, Dai Q, You Z. Discussion on molecular dynamics (MD) simulations of the asphalt materials. Adv Colloid Interface Sci 2022;299:102565.
[62] Kariznovi M, Nourozieh H, Abedi J. Measurement and correlation of viscosity and density for compressed Athabasca bitumen at temperatures up to 200°C. J Can Pet Technol 2014;53(06):330–8.
[63] Kariznovi M, Nourozieh H, Guan JGJ, Abedi J. Measurement and modeling of density and viscosity for mixtures of Athabasca bitumen and heavy n-alkane. Fuel 2013;112:83–95.
[64] Blom J, Soenen H, Van den Brande N. New evidence on the origin of 'bee structures' on bitumen and oils, by atomic force microscopy (AFM) and confocal laser scanning microscopy (CLSM). Fuel 2021;303:121265.
[65] Schuler B, Zhang Y, Liu F, Pomerantz AE, Andrews AB, Gross L, et al. Overview of asphaltene nanostructures and thermodynamic applications. Energy Fuel 2020;34(12):15082–105.
[66] Buch L, Groenzin H, Buenrostro-Gonzalez E, Andersen SI, Lira-Galeana C, Mullins OC. Molecular size of asphaltene fractions obtained from residuum hydrotreatment☆. Fuel 2003;82(9):1075–84.
[67] Sabbah H, Morrow AL, Pomerantz AE, Zare RN. Evidence for island structures as the dominant architecture of asphaltenes. Energy Fuel 2011;25(4):1597–604.
[68] Zhao T, Li X, Zhao H, Li M. Molecular simulation of adsorption and thermodynamic properties on type II kerogen: Influence of maturity and moisture content. Fuel 2017;190:198–207.
[69] Wu J, Li H, Goodarzi F, Min X, Cao W, Huang L, et al. Geochemistry and depositional environment of the Mesoproterozoic Xiamaling shales, northern North China. J Pet Sci Eng 2022;215:110730.
[70] Li DD, Greenfield ML. Chemical compositions of improved model asphalt systems for molecular simulations. Fuel 2014;115:347–56.
[71] M. Ashrafi, Y. Souraki, H. Karimaie, O. Torsaeter, B. Bjorkvik, Experimental PVT Property Analyses for Athabasca Bitumen. Canadian unconventional resources conference. Alberta, Canada; 2011:15-17.